POLITECNICO DI MILANO
Dipartimento di Fisica

LUNDS UNIVERSITET
Institutionen för Fysik

FAST MARKING BY SOLID STATE LASER: DEVELOPMENT OF A LASER SOURCE OPTIMIZED TO THE HIGHEST PROCESS PRODUCTIVITY

Master's Thesis

by

Nicola Foresti

2012

Lund Reports on Atomic Physics LRAP-460

Thesis supervisor:

Prof. Stefano LONGHI (Politecnico di Milano)

Prof. Orazio SVELTO (Politecnico di Milano)

Prof. Claes-Göran WAHLSTRÖM (Lunds Universitet)

Supporting supervisor:

Ph.D. Eng. Giovanni SCOTTI (SEI S.p.A.)

A Giovanna e Mario,
che se lo meritano davvero

Alla Libertà,
il bene più prezioso

Alla Consapevolezza,
lo strumento più utile

To Giovanna and Mario,
who really deserve it

To Freedom,
the most valuable asset

To Awareness,
the most useful tool

Till Giovanna och Mario,
som verkligen förtjänar det

Till Frihet,
den mest värdefulla tillgången

Till Medvetenhet,
den mest användbara verktyg

Abstract

In the past decades, the laser technology market for industrial material processing has grown by double digits. Nowadays, material processing by high power laser represents the almost irreplaceable solution for many needs. The company SEI S.p.A., based in Curno, Italy, requested a solid-state laser suitable for fast marking application. A Nd:YVO_4 crystal in end-pumped configuration was chosen in order to guarantee high performances, high quality and low cost. A study of the resonating cavity was made and thermal lensing was taken into account. The original solution here adopted, i.e., a low-doped (0.2 at. %) and relatively long (10 mm) crystal, allowed to reduce damaging thermal effects and to reach up to 17 W power in CW operation. Finally, a laser with quality factor $M^2 = 1.8$ and peak powers of 9 kW at 50 kHz in Q-switched regime was realized. This first prototype was then improved and today commercialized under the name *"Laser^3"*. More than 200 units have been sold so far.

Estratto in lingua italiana

Questo lavoro di tesi è stato svolto presso l'azienda SEI S.p.A. di Curno, in provincia di Bergamo, dal marzo 2007 al novembre 2008. La SEI S.p.A. realizza macchine laser per applicazioni industriali, in particolare taglio e marcatura di una svariata gamma di materiali. I laser utilizzati in SEI sono di quattro tipi: CO_2, Nd:YAG, UV ed in fibra. Di questi, i laser in Nd:YAG sono assemblati internamente, mentre i restanti sono acquistati da fornitori terzi. Scopo di questo lavoro è realizzare una sorgente laser a stato solido, pompata a diodi, che sia adatta per applicazioni di marcatura di precisione, alta qualità ed alta produttività. L'azienda richiede che vengano soddisfatti i seguenti requisiti:

- Una potenza in uscita di almeno 10 W in regime continuo
- Un modo laser con $M^2 < 2$
- Impulsi brevi ad alta ripetibilità in regime di Q-switch
- Raffreddamento ad aria
- Dimensioni compatte
- Alta affidabilità per utilizzo in ambito industriale

Si è scelto di sviluppare una sorgente in Nd:YVO_4 in configurazione a pompaggio longitudinale. Il pompaggio longitudinale garantisce un'alta qualità del fascio laser, mentre la scelta del cristallo in vanadato soddisfa le necessità di lavoro ad elevata frequenza di ripetizione degli impulsi. Lo scopo è realizzare una sorgente che abbia dei vantaggi evidenti rispetto ai più diffusi laser in fibra, come, per esempio, la possibilità di effettuare scale

di grigi, maggiore irradianza e costo inferiore. Sono state inoltre valutate le potenzialità di un cristallo in Nd:$GdVO_4$, che presenta interessanti proprietà fisiche, ma di cui ci sono pochi studi in letteratura.

Questo lavoro è strutturato in sette capitoli. Dopo il capitolo introduttivo, i capitoli 2 e 3 descrivono lo stato dell'arte nella tecnologia laser per marcatura. Il quarto capitolo è una rielaborazione di articoli di letteratura riguardo lo studio teorico di laser a stato solido. Gli ultimi tre capitoli descrivono il lavoro sperimentale ed i risultati ottenuti.

Il capitolo 2 descrive i principali vantaggi della marcatura laser rispetto le tecnologie tradizionali. Vengono spiegati i principi fisici che sottostanno al processo di marcatura. Partendo da considerazioni empiriche, vengono estrapolati i parametri fisci ottimali per un marcatore laser.

Il terzo capitolo descrive brevemente i laser più comuni per applicazioni di marcatura, cioè, i laser a CO_2, in fibra ed a stato solido. Di quest'ultima categoria in particolare vengono descritti e paragonati più in dettaglio i cristalli di Nd:YAG, Nd:YVO_4 e Nd:$GdVO_4$. Inoltre, vengono descritte alcune tecniche di pompaggio ottico, e si descrive il funzionamento dei diodi laser. Infine, date le considerazioni precedenti, si compie la scelta sulla tipologia di laser da sviluppare.

Nel quarto capitolo viene presentata un'analisi teorica dei laser a stato solido pompati longitudinalmente. Obiettivo dell'analisi è di individuare i parametri ottimali per massimizzare l'efficienza ottica e la qualità del fascio. Il design del risonatore viene inoltre studiato, tenendo in considerazione il fenomeno della lente termica. Si compie una analisi per il calcolo della stabilità e sensitività della cavità risonante.

Il capitolo 5 si concentra sulla realizzazione della sorgente. L'analisi teorica del capitolo quarto è applicata al caso pratico. In primo luogo, il diodo di pompaggio viene scelto e caratterizzato. Di seguito, i parametri ottimali per l'accoppiamento del fascio di pompa sono derivati dalla qualità del fascio di pompa stesso. Successivamente, vengono stimate la stabilità e la sensitività del risonatore. Infine, viene compiuta una scelta sulle proprietà del mezzo attivo, con lo scopo di minimizzare gli effetti termici.

Nel capitolo 6 vengono elencati i risultati sperimentali. Inizialmente viene realizzato un sistema raffreddato ad acqua, dopodichè, lo stesso sistema

viene convertito con raffreddamento a celle di Peltier, al fine di valutare le differenze di prestazione. Si vede come i due sistemi abbiano efficienze ottiche simili, attorno al 64%. Viene introdotta una correzione sperimentale alla formula di Innocenzi per il calcolo della focale termica, in quanto i valori predetti non si avvicinano alle misure sperimentali. La qualità del fascio laser è ritenuta accettabile ($M^2 = 1.8$) e vengono proposte soluzioni per migliorare ulteriormente questo valore. Viene sperimentato anche un cristallo di Nd:$GdVO_4$, che mostra però prestazioni inferiori rispetto al vandato. Infine, vengono confrontate le potenze di picco di diverse sorgenti laser, e si evidenzia come il vanadato fornisca le potenze maggiori ad alte frequenze.
Nel capitolo 6 vengono discussi i risultati e gli sviluppi futuri. Si sottolinea come sia stato possibile raggiungere un'emissione di 17 W in continua in configurazione end-pumped grazie all'uso di un cristallo lungo ed a basso drogaggio. Un ulteriore sviluppo del prototipo iniziale ha condotto alla commercializzazione di un sistema laser da marcatura, compatto, integrato, raffreddato ad aria, chiamato *Laser*^{3}, con potenza di uscita di 12 W ed $M^2 < 1.5$. Poco dopo è stato realizzata ed immessa sul mercato la versione potenziata a 20 W. Ad oggi, SEI ha venduto più di 200 *Laser*^{3} in tutto il mondo e sono in fase prototipale una versione da 30 W ed un laser verde generato tramite seconda armonica da questa stessa sorgente (vedere il lavoro di tesi di M. Epis [1]).

Populärvetenskaplig sammanfattning

Föreliggande arbete utfördes vid SEI SpA i Curno, Bergamo, Italien, från mars 2007 till november 2008. SEI S.p.A. tillverkar lasermaskiner för industriella tillämpningar, huvudsakligen märkning och kapning av en mängd olika material. Lasermaskiner som produceras av Sei SpA utnyttjar fyra olika typer av laserkällor: CO_2, Nd:YAG, UV och fiberlasrar. Bland dessa köps CO_2, UV och fiberlasrar av andra tillverkare, medan Nd:YAG källor monteras internt.
Syftet med arbetet är att utveckla en diodpumpad solid-state laser, som ska kunna tilllämpas för högprecisions lasermärkning, ha hög kvalitatet oh hög produktivitet. Den nya lasern ska uppfylla ett antal krav:

- En utgångseffekt av minst 10 W i kontinuerlig våg
- En låg ordningens strölmod: minst $M^2 < 2$
- Korta pulser med hög repeterbarhet i Q-switchad mod
- Luftkylning
- Kompakt format
- Industriell tillförlitlighet

Den valda lösningen är att utveckla en end-pumpad Nd:YVO_4 laserkälla, som tillämpas bland ett antal tillverkare och är känd som en effektiv lösning. Målet är att utveckla en källa med en rad viktiga fördelar jämfört med de idag mer använda fiberlasrarna, som t.ex gråtonskapacitet, högre irradians

och lägre kostnad. Den nya produkten kommer att tillåta SEI SpA att gå in i en växande marknad och konkurrera med andra företag som redan erbjuder lösningar för de tillämpningar som beskrivs ovan. Nd:$GdVO_4$ kommer också betraktas som en alternativ värd på grund av dess lovande fysikaliska egenskaper.

Denna rapport är uppdelad i sju kapitel, där det första kapitlet består av denna introduktion. Det andra och tredje kapitlet beskriver state-of-the-art inom lasermärkningsteknik. Kapitel fyra är en sammanfattning av artiklar som finns i litteraturen om teoretiska studier av solid-state laserkällor. De tre avslutande kapitlen beskriver det experimentella arbetet och dess resultat.

I kapitel 2 är de viktigaste fördelarna med lasermärkning jämfört med traditionella metoder beskrivna. De fysikaliska principerna bakom lasermàrkningsprocessen förklaras och tekniker för strålleverans visas. I detta kapitel beskrivs hur optimala fysiska parametrar för en industriell lasermarkör härrör från fysiska och empiriska överväganden.

Det tredje kapitlet beskriver kortfattat de vanligaste laserkällorna för märkningstillämpningar, dvs CO_2 lasrar, fiberlasrar och solid-state lasrar. Här beskrivs solid-state lasrar, där tre laserkristaller, Nd:YAG, Nd:YVO_4 och Nd:$GdVO_4$, beskrivs och jämförs mer i detalj. Dessutom behandlas ett antal tekniker för optisk pumpning, tillsammans med en beskrivning av laserdioder, som idag är föredragna anordningar för solid-state laser pumpning. Slutligen är ett val av den typ av laser som skall utvecklas motiverat på grundval av de tidigare beskrivna diskussionerna.

I det fjärde kapitlet är en teoretisk analys för en end-pumpad solid-state laser presenterad. Målet med analysen är att hitta de designparametrar som maximerar källans effektivitet och kvalitet. Resonatorns design är också beaktad och fenomenet termisk linsverkan övervägs. En teoretisk analys av resonatorstabilitet och känslighet presenteras.

Kapitel 5 fokuserar på källans design. Den teoretiska analysen i kapitel 4 är här applicerad på ett verkligt exempel och beräkningar utförs i syfte att maximera laserns kapacitet. Först väljs och karakteriseras en pumpanordning. Det andra steget är att finna den bästa kopplingsmetoden från en teoretisk och praktisk synvinkel. Tredje steget är att värdera resonatorns stabilitet och känslighet. Slutligen görs ett val av det aktiva mediets egen-

skaper, i syfte att minimera termiska effekter.

I kapitel 6, visas ett flertal gjorda mätningar med den nyutvecklade lasern. En vattenkyld uppsättning görs, tillsammans med en termoelektrisk kylning (TEC), för att ha jämförbara data och kunna utvärdera effektiviteten av TEC lösningen. I själva verket är det TEC uppsättningen nästan lika effektiv som den vattenkylda uppsättningen. En maximal uteffekt på 19,1 W registrerades med en 64% lutningseffektivitet. En experimentell korrigering av Innocenzis formel föreslås, eftersom det framgår av experimentella data att de teoretiska beräkningarna, under vissa omständigheter, inte är nära de uppmätta värdena. Strålkvalitet anses vara godtagbar ($M^2 = 1.8$) och lösningar föreslås för att förbättra den. Gadolinium som värd har också utvärderats, men befanns inte vara så lämpliga som vanadat kristall. Slutligen jämfördes toppeffekter av flera laserkällor och vanadatkristallen visar sig vara det bästa valet för de uppsatta målen.

I kapitel 7 är slutsatser och framtida utveckling beskriven. Detta arbete visar hur det är möjligt att nå hög effekt i end-pumped konfiguration tack vare långa och lågdopade aktiva medier. I själva verket erhölls en luftkyld laser med en uteffekt av upp till 17 W i kontinuerlig våg operation. Samma laser inställd på 10 W uteffekt visade en $M^2 = 1.8$ i pulsad mod, med 9 kW puls toppeffekt vid 50 kHz repetitionsfrekvens. Det visas också hur Innocenzis formel inte är tillräckligt exakt, under vissa omständigheter, för att förutsäga den termiska linsbrännvidden.

Vidareutveckling av den första prototypen ledde snabbt till en kommersiella produkt med namnet *"Laser^3"*, en 12 W källa, som i själva verket är ett litet, kompakt och komplett lasermärkningssystem. Kort därefter togs det fram en 20 W lösning som också släpptes ut på marknaden. Numera (2012) har SEI sålt mer än 200 enheter över hela världen. En 30 W prototyp är under utveckling, medan de viktigaste insatserna nu har flyttas över till utvecklingen av en grön laser utnyttiande frekvensdubbling. Förstudie har redan utförts, som visar lovande resultat (se examensarbetet av M. Epis [1]).

Acknowledgements

My main thanks go to Giovanni Scotti and Fausto Cavenati. Their help and support throughout the duration of this thesis work and, especially, after it, was decisive. Their technical competence and their human qualities are to me of great value.

I want also to thank the whole SEI S.p.A. and especially my colleagues of the Demo Room, for taking me as part of their team. I now have the chance to do a job that I like in a stimulating environment.

Many thanks to Martin and Tommaso, who's job is in here as well.

Finally, I probably have to thank all the "Knights Shovers" (*Spingitori di Cavalieri*) who never lost the chance to remember me I hadn't completed my studies...

Contents

List of Tables

List of Figures

Chapter 1

Introduction

The present work was carried out at SEI S.p.A. in Curno, Bergamo, Italy, from March 2007 to November 2008. SEI S.p.A. manufactures laser machines for industrial applications, mainly marking and cutting of a wide range of materials. The laser machines produced by Sei S.p.A. make use of four different kind of laser sources: CO_2, Nd:YAG, UV and fiber lasers. Among these, CO_2, UV and fiber lasers are purchased by other manufacturers, while Nd:YAG sources are assembled internally. Purpose of this work is to realize a diode pumped solid-state laser suitable for high precision laser marking applications, such as laser trimming, solar cells manufacturing, coatings and oxides ablation, thermoplastic marking. The new laser shall fulfill a number of requirements:

- An output power of at least 10 W in continuous wave operation
- A low order mode beam: at least $M^2 < 2$
- Short pulses with high repeatability in Q-switched regime
- Air cooling
- Compact size
- Industrial reliability

The choice is to develop an end-pumped Nd:YVO_4 laser source, which is known to be an effective solution, adopted by other few manufacturers.

The goal is to realize a source with important advantages over the more widespread fiber lasers, such as graytones capability, higher irradiance, lower cost. The new product will allow SEI S.p.A. to enter in a growing market and to compete with other companies that already offer solutions for the applications described above. Nd:$GdVO_4$ will also be considered as an alternative host, due to its promising physical properties.

This work is structured into seven chapters. The first chapter is this introduction. The second and third chapters describe the state-of-the-art in laser marking technology. Chapter four is a report of articles present in literature regarding the theoretical study of solid-state laser sources. The last three chapters describe the experimental job and its achievements.

In chapter 2 the main advantages of laser marking over traditional processes are described. The physical principles behind laser marking process are explained and techniques for beam delivery are shown. In this chapter optimal physical parameters for an industrial laser marker are derived from physical and empirical considerations.

The third chapter briefly describes the most common laser sources for marking applications, i.e., CO_2 lasers, fiber lasers, and solid-state lasers. Regarding solid-state laser, three laser crystals, Nd:YAG, Nd:YVO_4 and Nd:$GdVO_4$, are described and compared more in detail. Moreover, a few techniques for optical pumping are described together with a description of laser diodes, which are nowadays the elected devices for solid-state laser pumping. Finally, a choice on the kind of laser to be developed is taken, based on the previous discussions.

In the fourth chapter, a theoretical analysis for an end-pumped solid-state laser is presented. Goal of the analysis is to find the design parameters that maximize the source efficiency and quality. The resonator design is also taken into account and the phenomenon of thermal lensing is considered. Theoretical analysis on resonator stability and sensitivity are presented.

Chapter 5 is focused on the source design. The theoretical analysis of chapter 4 is here applied to a real example and calculations are performed in order to maximize the laser performances. At first, a pumping device is chosen and characterized. Second, the best coupling approach is evaluated from a theoretical and practical point of view. Third, resonator stability

and sensitivity are evaluated. Finally, a choice on active medium properties is done, with the aim of minimizing thermal effects.

In chapter 6, several measurements on the newly developed laser are performed. At first, a water-cooled set-up is realized together with a thermoelectric cooled set-up, in order to have comparable data and evaluate the efficiency of the TEC solution. In fact, the TEC set-up is nearly as efficient as the water cooled set-up. A maximum output power of 19.1 W was recorded, with a 64% slope efficiency. An experimental correction to Innocenzi's formula is proposed, as it is evident from experimental data that the theoretical calculations, under certain circumstances, are not close to the measured values. Beam quality is found to be acceptable ($M^2 = 1.8$) and solutions are proposed to improve it. Gadolinium host was also evaluated, but found to be not as suitable as the vanadate crystal. Finally, the peak powers of several laser sources are compared and the vanadate crystal is found to be the best choice for the declared goals.

In chapter 7, conclusions and future development are described. This work shows how it is possible to reach high power in end-pumped configuration thanks to long and low-doped active media. In fact, an air-cooled laser with an output power of up to 17 W in continuous wave operation was generated. The same laser tuned to 10 W output showed an $M^2 = 1.8$ in pulsed regime, with 9 kW pulse peak power at 50 kHz repetition frequency. It is also shown how Innocenzi's formula is not sufficiently accurate, under certain circumstances, to predict the thermal lens-focal length.

Further development of this first prototype quickly led to the commercial product called *"Laser^3"*, a 12 W source, that is in fact a small, compact and complete laser marking system. Shortly after, a 20 W solution was also realized and put on the market. Nowadays, SEI sold more than 200 units worldwide. A 30 W prototype is under development, while the main efforts are now moved to the development of a green laser by second harmonic generation. Preliminary study has already been performed, showing promising results (see the master thesis by M. Epis [1]).

Chapter 2

Industrial Laser Marking

In the past decades, the laser technology market for industrial material processing has grown by double digits [2]. With improved beam sources, expanded scope and optimization of system concepts, lasers have become efficient, reliable manufacturing tools in a variety of sectors. Nowadays, material processing by high-power laser represent the almost irreplaceable solution for many needs. In particular, marking and engraving systems with CO_2 and solid-state laser sources have a great diffusion and development. Thanks to their versatility, they often are a better choice than other traditional processes.
Section 2.1 introduces the laser marking process in industry, while section 2.2 describes the physical processes behind laser marking. In section 2.3 a quick description of a beam delivery system for laser marking is given.

2.1 Laser Marking Applications

Laser marking applications became more and more popular in several different industrial and artisan activities. By means of systems equipped with laser sources and tools for focusing and positioning the laser beam, it is possible to engrave or at least make visible marks on almost every sort of material, being organic, plastic, ceramic or metallic. This provides an answer to the typical needs of both industrial and artisan fields: at one hand the need of product certification, traceability and anti-counterfeiting;

on the other hand, customization, decoration and embellishment of finished and unfinished products. For example, in many productive environments with needs of part coding, laser technology offers, in the medium-long term, undoubted advantages both economical and technical (indelible traces, no toxic materials...) compared to conventional ink-jet, pad printing and inks for UV-polymerization. Moreover, beside this applications, special processes with a high added value, (e.g., in fields like micro-mechanics, electronic and photovoltaic industry, composite material die-cutting) are becoming more and more important thanks to a tool, the laser, very different from a typical mechanical tool.
The most appealing features of laser technology can be synthesized in the following points:

1. Indelible effect of the laser mark
2. High speed, accuracy and repeatability
3. Quick reconfigurability
4. Absence of mechanical contact
5. Low energetic transfer on the workpiece
6. Versatility and flexibility
7. Low cost in the mid-long term
8. Ease of integration on every productive line

Thanks to the intrinsic versatility, the application fields of laser marking are extremely wide. It is possible to mention:

- Electronic and electromechanical components, for logos and alphanumeric codes marking. These are globally the fields where the highest number of laser marking units are used. Generally integrated in continuous working production lines, they operate in automatic mode
- Mechanical tools, for logos and alphanumeric codes marking. Here there are generally stand-alone systems with automations for tool loading, unloading and handling. These might also be on-line systems

- Items in the fashion industry, for marking decorations, writings, logos and brands. Generally stand-alone machines with limited automation capabilities
- Household articles, for marking decorations, writings, logos and brands. Generally stand-alone machines with limited automation capabilities
- Mechanical, hydraulic and pneumatic components, for alphanumeric codes marking. Generally stand-alone machines with limited automation capabilities
- Components for the automotive industry, for logos and alphanumeric codes marking. Generally placed on continuous working production lines, they work in automatic mode
- Items made of organic or plastic materials. The material marking, engraving or ablation by laser is generally the main process that leads to the end-product
- Packaging, for alphanumeric codes, barcodes or logos marking. Generally on-line machines with high throughput and high integration

Depending on the application field, the level of productivity and handling demanded, laser machines present different configurations for different automation, attachments, options, interfaces. However, they always rely on a basic scheme: a source, a galvanometric beam deflection system, focusing optics, command and control electronics.
The laser sources used in the great majority of the applications are of two large families:

- gas sources, namely CO_2, emitting in the infrared region (10600 nm)
- "solid state" sources, emitting mainly in the near infrared (1050-1080 nm)

Except for packaging applications, the second kind of laser is the most widely used in industrial applications.
The laser developed in this work falls into this technological field.

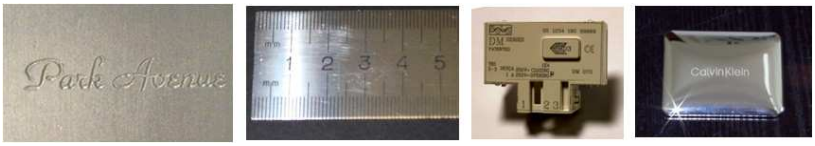

Figure 2.1: Photos with examples of laser marking by material removal, surface browning, burning and oxidation

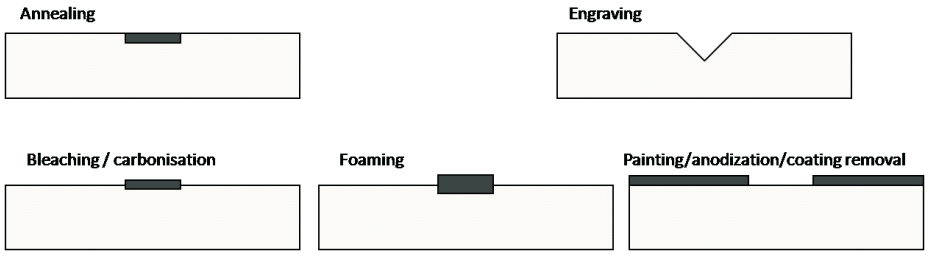

Figure 2.2: Schematic representation of laser interaction with surfaces.

2.2 Physics of the Laser Marking Process

The marking process by means of laser light falls in the field of radiation-matter interaction. Superficial marking with laser light can be defined as a process that by locally releasing energy on a surface, modifies its appearance permanently. The interaction can show mechanical (material ablation), thermo-physical (changes in the superficial crystalline lattice, browning) or chemical (combustion, oxidation and several other reactions) effects depending on the processed material and on the radiation properties. The action is effective when the laser beam is focused on the surface and moved over it. Therefore, the mark is obtained by a sort of "laser tool" of micrometric dimensions (typically 20-200 μm) driven on the workpiece according to a predefined geometry. Normally the laser beam is made of short pulses repeated at high frequency, focused and overlapped on the material in order to form lines or fillings. There exist, anyway, special applications where a continuous emission is preferable, but these represent a meager minority.

Every material can absorb more or less efficiently laser light at certain wavelengths, depending on its atomic/molecular structure, its surface finish-

ing and its temperature. The higher the absorption, the higher the machinability. The vast majority of the material is sensitive to the wavelength of two kinds of laser sources: solid state, with wavelength around 1060-1080 nm, and CO_2, with wavelength 10600 nm.

CO_2 laser action is nearly always thermal or chemical, giving vaporization or burning. CO_2 lasers are normally used with organic and polymeric materials. Also metallic materials can be processed when anodizations or varnishing are present.
The interaction of solid state laser with giant pulses (Q-switched or MOPA) is more complex. These lasers emit very short length pulses (nanosecond range) capable of extremely high and localized thermal shocks on the material.

- On metals, depending on the material, a visible mark can be obtained mainly by three techniques. Each technique is different due to the thermal gradient produced on the material surface: (1) superficial micro-browning, (2) localized micro-melting, (3) material micro-vaporization. These three phenomena always take place together; the material structure and the interaction level determine the predominance of one effect over the others. Superficial browning is generally carried out on metals such as steel alloys, titanium, ferrous metals. Suitable filling patterns and energetic levels allow to create coloring in different shades (black, brown, blue, fuchsia, violet, red, yellow, etc.). In case of superficial treatments like chromium plating, anodizations or superficial layers of any kind, the marking is made removing by vaporization the superficial coating up to 10 μm per pass. Depending on the substrate, high visible contrast effects together with high process speeds are obtained. Micro-melting is often associated to oxidation phenomena and gives the main effect of desired contrast on precious metals. Lastly, micro-vaporization on metal is used to create light engraves (0.5-10 μm) or, by suitable strategies for material removal, real engraves two- or three-dimensional (for engraving or molds).

- In case of polymers without additives, the contrast effect is given by micro-vaporizations or micro-carbonizations capable of material re-

CO_2 Lasers only	**CO_2 and/or SS Lasers**	**SS Lasers only**
Glass compounds	PTFE, PP, Polypropylene	Precious Metals
Crystal and amorphous glasses	Polycarbonate, PVC	Generic Metals
Organic materials	Anodized/coated metals	Galvanic Coated Metals
Synthetic textiles	Rubber, Textiles	

Table 2.1: Example of processable materials with Solid State and CO_2 lasers

moval or also "bubbles" in the interaction area. Depending on the material the effects can be aesthetically pleasant (e.g., polycarbonate or PVC) or rough.

- Other plastic polymers deserve a separate treatment. Thermosensitive additives are manufactured by well-known chemical industries: the addition in small quantities of these additives do not modify the polymer physical and chemical properties (e.g., electrical insulation and mechanical strength), but allows high quality laser marking on materials generally not sensitive to laser light or with tendency to carbonization. The resulting effect is a permanent color change of the processed surface.

In table 2.1 is presented a short summary of materials processable with the laser sources discussed so far.

It is not easy to perform a quantitative analysis of the industrial laser marking or engraving process, due to the multiple thermodynamical phenomena which might or might not take place. It is however possible to discuss three aspects, normally correlated:

1. the capability of performing the processes described above
2. the process speed (and therefore the productivity)
3. the process uniformity in space and time

In physical terms, the first component is expressed by a quantity called irradiance, indicating the energy transferred to the material in the time range of a laser pulse. It is conventionally measured in W/cm^2. Irradiance

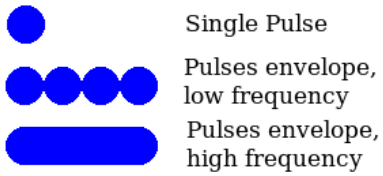

Figure 2.3: Representation of laser pulses shot on a surface at constant speed and different frequency

can be expressed by the following expression, comprehensive of both the beam physical parameters and of the focusing system:

$$\text{Irradiance} = \frac{E_\text{n}}{t_\text{p}} \cdot \frac{1}{\pi w^2} = \frac{E_\text{n}\pi}{t_\text{p}\lambda^2} \cdot \left(\frac{D}{f}\right)^2 \cdot \frac{1}{(M^2)^2} \tag{2.1}$$

where w is the beam radius at focal point, E_n is the energy per single pulse, t_p is the pulse length in time, λ is the radiation wavelength, f the focal length of the flat-field theta lens, D the pupil radius at the scanning system entrance and M^2 the beam quality factor, strictly correlated to the source brightness. From literature and from SEI's several years of on-field experience it resulted evident how the great majority of industrial processes requires an irradiance between 10^4 and 10^8 W/cm^2 per pulse. Therefore, the "perfect" laser marker must guarantee and properly control the pulses irradiance in this range. Note that the formula consider parameters related to the focusing optics (f and D), the beam quality (M^2) and the pulse energy (E_n). The optimum lasers will have a low M^2 (the theoretical limit is 1), high E_n and short t_p . On the other hand , a high productivity (point 2 above) is given by the capability of having such pulses at high repetition rates, i.e. at high frequency. Moreover, the beam delivery system must be sufficiently fast and accurate, giving a limit on the lens pupil dimension D, shortly related to the inertia, i.e. the dynamics, of the scanning mirrors.

The third aspect is related to the marking uniformity, in terms of space and time. In space, pulse shape and symmetry are important together with pulse similarity on the whole working plane. In time, it means that the

Irradiance	$10^4 - 10^8$ W/cm^2
Pulse Energy (dependent on f)	0–2.5 mJ
Pulse Width	5–50 ns
Pulse Repetition Frequency	0–100 kHz
Pulse Energy Instability	$< 5\%$
Pulse Temporal Instability	$< 5\%$
Pulse Shape	Gaussian or quasi-Gaussian
M^2	< 1.5
Spot Diameter	20–100 μm
Focal Distance	100–400 mm
Angular Velocity	0–100 rad/s
Angular Acceleration	Up to 300000 rad/s^2

Table 2.2: Optimal values for laser marking, industrial applications (courtesy of SEI)

pulses must be similar in the short and in the long term range, i.e. after a few microseconds or after thousands working hours. This is essential in order to have processes of a predictable quality. This depends certainly on the material uniformity but also on the system capability to emit and place pulses of the desired irradiance with constant shape at every working frequency and energy. Physically, uniformity therefore depends on the pulses temporal and energetical stability and on the displacement accuracy in every working condition. Lastly, Gaussian or quasi-Gaussian distributions are to be preferred, being the mechanical action of the laser tool defined by the shape of the laser pulse. Therefore, it is evident how all the three aspects are strictly dependent on the source, the scanning system and the electronic control. The optimal result can be reached only with an integrated and synergic system.

In conclusion, optimal parameters for laser marking can be deduced from the preceding considerations and suitably summarized: see table 2.2. If we suppose we can focus the laser into a 60 μm wide spot, than it is easy to calculate that a 10 kW peak pulse is sufficient to have a 10^8 W/cm^2 irradiance on the material. A marking system with such characteristics can satisfy the great majority of the industrial needs, with high level productivity and quality execution. Purpose of this research is to develop a laser source

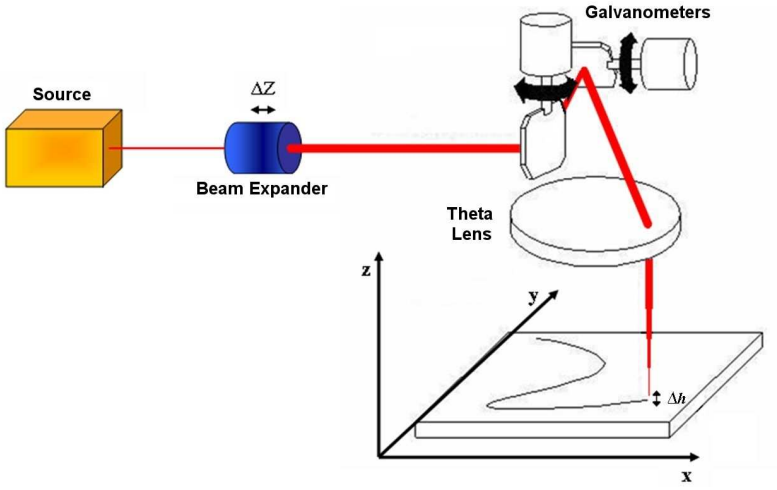

Figure 2.4: Scheme of a scanning head for laser marking

able to fully satisfy these requirements.

2.3 Scanning Head for Laser Marking

The great majority of the installed engraving systems make use of a scanning head of the type shown in figure 2.4, which performs a so-called *linear marking*. The beam coming out from the laser source is at first magnified by a beam expander and then deflected by two rotating mirrors with rotation axis perpendicular to each other. The rotation is driven by two motorized galvanometers, and the whole system is called *scanning head*. The beam then goes through a particular kind of lens called *theta lens* which has a planar focal surface. This set-up guarantees a very fast and responsive system, allowing the focal spot to be moved very rapidly and accurately. Moreover, by moving the beam expander on the beam axis, the focal plane can be moved in the vertical direction, allowing the engraving of 3D structures. The working area for these systems is generally limited to 200×200 mm, due to the high cost of the theta lenses.

Chapter 3

Sources for Laser Marking

Laser generation can take place within different material in different physical phases: solid, liquid or gaseous. A detailed description of the physical principles behind laser generation is not purpose of this work, we therefore redirect the reader to other books, such as, e.g., Principles of Lasers, by O. Svelto [3].

Different industrial applications require different kinds of laser beams, which may differ for the working regime (cw or pulsed), the output power (from a few watts up to several kilowatts), the radiation wavelength (from UV to infrared regions) and the shape and geometrical characteristics of the beam. Obviously, each laser source is characterized by specific features and is suitable for specific applications. Therefore, different sources are developed for different applications. Laser sources mainly used for marking applications are CO_2 lasers and solid-state (especially Nd:YAG) lasers. Fiber lasers also appeared on the market and are widely available. High speed and repeatability are the main requirements for marking applications, while laser beam quality becomes a critical point when it is necessary to realize small incisions with high precision. The most important laser technologies for industrial marking applications will be here briefly presented. In section 3.1 several kind of CO_2 laser sources are presented and their peculiarities described. In section 3.2 fiber lasers are discussed, while section 3.3 describes more accurately solid-state sources. Finally, in section 3.4 the reasons leading to the development of a longitudinally pumped solid-state

laser are discussed.

3.1 CO_2 Lasers

CO_2 lasers are the most widely used sources in industrial applications of the mechanical sector, mainly for cutting metallic and non-metallic materials, or engraving coated metals and organic materials. Output powers can vary from few watts up to more than 40 kW: typical powers for metal cutting are around 2.5 kW, while cuts on non-metallic materials make use of output powers ranging from 100 W to 1000 W. Moreover, thousands of low power lasers (output powers < 100 W) are sold every year for marking and coating-removal applications. The gain medium is the carbon dioxide molecule (CO_2), which is mixed with helium and nitrogen in a specific ratio to improve the system pump efficiency. Lasing action takes place at a wavelength of 10.6 μm, in the infrared region.

Laser sources commercially available and suitable for laser marking are:

- **glass sealed tube**: This is the oldest technology for CO_2 lasers. It simply consists in a glass tube containing the gas mixture and two electrodes placed at the tube sides. The source can work for more than 5000 hours before the gas mixture has to be replaced. Cooling is done by natural convection on the tube surface, therefore limiting the maximum output power to 200 W. Typical applications are marking and cutting of non-metallic materials such as cloths, leathers, paper, etc. Glass sealed tubes are a low-cost solution with a few drawbacks, such as short lifetime, low modulation capability, low pulsing capability and and generally low productivity.

- **slow axial flow**: the gas mixture is injected at one end of the tube and extracted at the other. The mixture is then cooled and re-injected in the tube. The speed of the gas mixture is ≈ 1 m/s and the output power range is 60-80 W per meter of length with high beam quality, even though temperature variations during the operation can lead to instability in the beam profile.

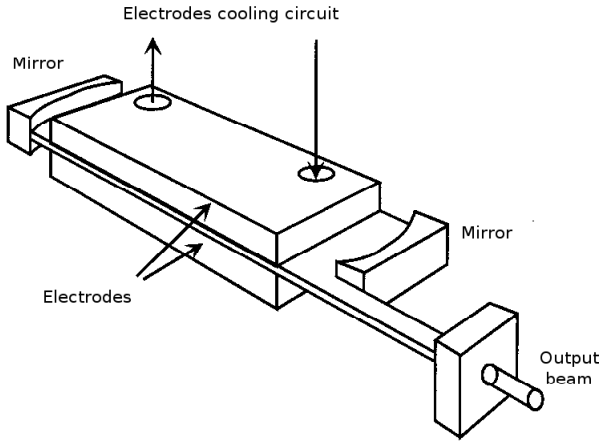

Figure 3.1: Schematic structure of a $C0_2$ laser slab source

- **metal sealed tubes RF excited** This are the most common laser tubes for output powers between few watts and several hundred watts. The gas mixture is contained in a metallic sealed tube and excited via radiofrequency discharges. The operation frequency can be very high, up to 200 kHz. These lasers are compact and rugged, and reach operation lifetimes of several thousands of hours.

- **slab**: these consist of a cavity with a parallelepipedal geometry (see fig. 3.1. The two wider faces of the cavity are the electrodes, cooled by convection. The cavity is confined by two mirrors, one of the two being smaller: from this aperture the laser beam is extracted. Maximum output powers reach 6 kW, the beam quality is improved with external optical elements. These slab sources offer the best output power/cost ratio, together with high pulsing capability, high power modulation capability, compact dimensions, high peak powers, excellent lifetime and reliability. Nowadays they are the most popular lasers in the range 100-5000 W.

The main limitation of CO_2 laser is represented by its wavelength, which is badly absorbed by metals and sometimes leads to a low focusability. This has two consequences: low marking resolution and the need for high power to reach the necessary intensity in the focal point. Consider, e.g, a CO_2 laser,

with 80 W output power and a beam diameter after the beam expander of 15 mm. If the beam is focused on the workpiece with a lens with 180 mm focal length, the spot size will result, at best [4]:

$$d_2 = \frac{4}{\pi}\frac{\lambda f}{d_1} = \frac{4}{\pi} \cdot \frac{10.6\,\mu\text{m} \cdot 180\,\text{mm}}{15\,\text{mm}} = 162\,\mu\text{m}$$

with an optical intensity $I = P/[\,\pi\,(d_2/2)^2\,] = 80\,\text{W}/[\,\pi\,(162/2\,\mu\text{m})^2\,] = 3.9\,\text{kW/mm}^2$. Consider now a Nd:YAG laser in the same conditions. Thanks to its wavelength at 1.064 μm, the spot on the workpiece simply becomes ten times smaller and by consequence the intensity is a hundred times higher, with great process enhancement. Clearly, the choice between a CO_2 laser or a solid state laser is, first of all, application driven, i.e., the CO_2 wavelength can be advantageous or just strictly necessary depending on the material to be processed (cfr table 2.1).

3.2 Fiber Lasers

In a fiber laser the active medium is the fiber core doped with a rare earth. Most commonly, this is a single-mode fiber made of silica. The pump beam is launched longitudinally along the fiber length and it may be guided by either the core itself, as occurs for the laser mode, or by an inner cladding around this core (double-clad fiber laser). The first solution requires a diffraction-limited pump source for efficient pumping. The second solution, illustrated in fig. 3.2, is more appropriate when high pump power is necessary. The core lies within a lower index inner cladding that in turn lies within an outer cladding of a yet lower index. Pump light can be end-launched into the inner cladding with a less stringent beam quality requirement than into the core. While propagating in the inner cladding, this pump light is progressively absorbed by the core. Laser light oscillation is not guaranteed by mirrors, but by two Bragg's gratings conveniently patterned in the fiber. Cladding-pumped Nd-doped fibers and Yb-doped ($\lambda = 1.08\,\mu$m) fibers with output powers of several watts are commercially available. In particular, Yb:glass fibers can guarantee high output powers ($\sim$ 300 W) with excellent beam quality. By the use of more fibers in par-

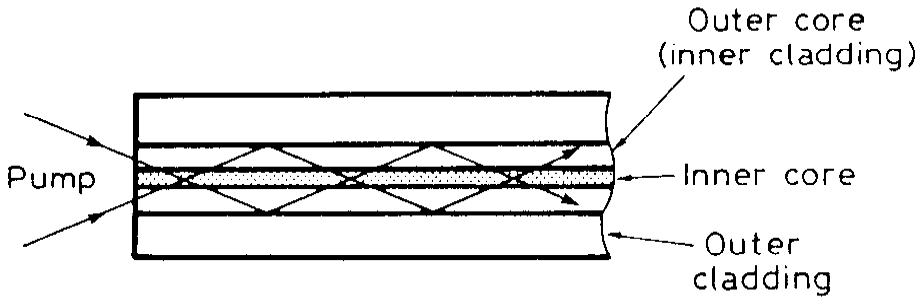

Figure 3.2: Scheme of a cladding pumping

allel, output powers up to 10 kW can be achieved. This makes the fiber lasers suitable for metal cutting applications. For marking applications, Q-switched or MOPA configurations are used. These are characterized by an excellent mode beam profile, high reliability and lifetime. The main limitations are the maximum energy per pulse (approx 1 mJ) and the pulses duration (hundreds of nanoseconds) that lead to low peak powers and therefore low attainable irradiance. Together with these physical limitations, the high cost of the system has also to be taken into account. Anyhow, their importance for industrial applications is rapidly growing.

3.3 Solid State Lasers

The term solid-state laser is generally reserved for laser having ions introduced as an impurity in an otherwise transparent dielectric-host material (in crystalline or glass form). Ions belonging to one of the series of transitions elements of the Periodic Table, in particular rare earth (e.g. Nd, Ho, Er, Yb) or transition-metal ions (e.g. Cr, Ti, Co, Ni), are generally used as the active impurities. For host crystals, either oxides, e.g., Al_2O_3, or fluorides, e.g., $YLiF_4$ (abbreviated YLF) are most often used. A suitable combination of oxides to form synthetic garnets, such as $Y_3Al_5O_{12}$ (abbreviated YAG: Yttrium Aluminum Garnet) or YVO_4 (Yttrium Orthovanadate) are often used.

Neodymium (Nd) lasers are the most popular type of solid-state laser.

	ρ (g/cm^3)	n @ 1064 nm	K$_c$ (W/K m)	σ_e ($10^{-19} cm^2$)	τ (μs)
Nd:YAG	4.56	1.8197	14	2.8	230
Nd:YVO$_4$	4.22	n$_o$ = 1.9573 n$_e$ = 2.1652	5.23 $\parallel n_e$ 5.1 $\perp n_e$	14.1 [6]	84.4 [6]
Nd:GdVO$_4$	5.47 [7]	n$_o$ = 1.9854 [7] n$_e$ = 2.1981 [7]	11.7 [7]	10.3 [6]	83.4 [6]

Table 3.1: Summary of physical properties of Neodymium-doped crystals. ρ is the crystal density, n the refractive index, ordinary or extraordinary, K$_c$ the thermal conductivity, σ the stimulated emission cross-section and τ the fluorescence lifetime.

The host medium is often a crystal of YAG in which some of the Y^{3+} ions are replaced by Nd^{3+} ions. Nd:YAG, because of its high gain and good thermal and mechanical properties, is by far the most important solid-state laser for scientific, medical, industrial and military applications. Another common host medium is vanadate, in particular Nd:YVO$_4$, which has become a very attractive material for small diode-pumped lasers because of its large emission cross section and strong absorption at 809 nm. A popular host material for Nd^{3+} ions is GdVO$_4$, which has been developed by Zagumennyi et al. [5]. Compared with Nd:YAG and Nd:YVO$_4$ crystals, Nd:GdVO$_4$ has a larger emission cross section at 1.06 μm and a larger thermal conductivity. A few physical properties of the three crystal are summarized in table 3.3 for a quick comparison.

Solid-state lasers are extremely important in industrial applications. The big advantage over other laser sources is the capability to Q-switch, i.e., quickly modulate the cavity losses, with generation of laser pulses with a duration comparable to the photon decay time (in few tens of nanoseconds range) and high-peak power (in the megawatt range). This allows a material ablation in a very quick and precise way, and makes solid-state lasers very suitable for fast marking applications.

3.3.1 Active Media

Laser crystals are typically single crystals (monocrystalline material) mainly grown with the Czochralski technique. Sometimes, composite crys-

tals (i.e. crystals with spatially varying chemical concentration) are used for several different reasons. Quite different geometric forms can be used:

- A common form is that of a cuboid. The crystal can e.g. be a thin coplanar plate, with transverse dimensions (perpendicular to the laser beam) and a thickness of a few millimeters. It may be oriented for near perpendicular incidence of the laser beam, or at Brewster's angle. It can be fixed in some solid mount which also acts as a heat sink. Larger crystals are usually used for side pumping e.g. with high-power diode bars.

- Slab lasers are based on relatively flat slabs, which may or may not be of cuboid form.

- Many side-pumped lasers use relatively long cylindrical laser rods. Particularly for lamp-pumped lasers, rod length can be several centimeters, whereas the rod diameter is much smaller (a few millimeters).

- Thin-disk lasers require a disk, often with circular cross section, having a thickness of only 100-200 μm and a relatively high doping concentration.

For given dopant and host medium, the doping concentration is the most important parameter. Other issues of interest are the uniformity of doping (influencing the tendency for quenching), the level of impurities (e.g. unwanted other rare-earth ions), and the optical homogeneity. Several of these factors influence the absorption and scattering losses of the material, and/or the strength of thermal lensing. Of course, it is very desirable that a given crystal quality is consistently produced, although different laser designs can have a quite different sensitivity to material parameters. A high surface quality is also important. Specifications of surface flatness are often better than $\lambda/10$. This helps to avoid both scattering losses and wavefront distortions which can degrade the laser's beam quality. Finally, a high degree of end face parallelism can be important for avoiding changes of beam direction in the crystal. Three hosts for neodymium laser-active dopant will be further analyzed in the following sections.

3.3.1.1 Nd:YAG

Nd:YAG possesses a combination of properties uniquely favorable for laser operation. The YAG host is hard, of good optical quality, it has a high

thermal conductivity and its structure is stable from the lowest temperature up to the melting point [8].

In Nd:YAG laser action can be obtained at several wavelength, but the most widely used transition is the ${}^4F_{3/2} \rightarrow {}^4I_{11/2}$ which makes the laser work in a four-level scheme and gives a lasing wavelength of 1.064 μm. Neodymium concentration by atom percent in YAG has been limited to 1.5%. Higher doping levels tend to shorten the fluorescent lifetime, broaden the linewidth and cause strain in the crystal, resulting in poor optical quality. Nd:YAG lasers can operate either cw or pulsed, and can be pumped by either a lamp or by diode lasers, with a slope efficiency which is much higher for diode pumping. Output powers can vary from a few watt up to 6 kW. Typical values are 500 W of average output power in pulsed regime and 1 kW in cw [4]. Nd:YAG lasers are widely used in a variety of applications, including material processing, such as drilling, welding and engraving and medical applications such as coagulation and tissue evaporation. In particular, side-pumped Nd:YAG laser rods are successfully used as sources for laser engraving. Output powers up to 100 W can be reached in multimode cw operation. When high beam quality is required, single mode operation is obtained by introducing a small aperture in the cavity, which reduces the laser quality factor M^2 at the cost of lower output power. Problems arise in fast marking: it has been shown that for high working frequencies the variability of the pulses greatly increase and a considerable percentage of pulses do not take place at all [9].

3.3.1.2 Nd:YVO_4

Neodymium-doped yttrium vanadate has several spectroscopic properties that are particularly relevant to laser diode pumping. The two outstanding features are a large stimulated emission cross section which is five times higher than Nd:YAG, and a strong broadband absorption at 809 nm. The gain coefficient of Nd:YVO_4 is about three time larger than that of Nd:YAG, which makes Nd:YVO_4 lasers less sensitive to cavity losses, and, together with the strong absorption of diode pump radiation, require crystals only a few millimeters in length. The vanadate crystal is naturally birefringent

and laser output is linearly polarized. The host has, on the other side, several drawbacks, the principal one is a shorter excited state lifetime than Nd:YAG, which limits the capability in Q-switched operation. Furthermore, the thermal conductivity is half as high as in Nd:YAG, and this results in worst thermal properties, shorter thermal lens-focal length and difficulties in heat removal. The properties of Nd:YVO_4 can best be exploited in an end-pumped configuration and a number of commercial laser systems are based on fiber-coupled diode arrays pumping a small vanadate crystal. Nd:YVO_4 is the material of choice for low-medium power ($\sim$ 5-20 W cw) end-pumped lasers. Impressive overall efficiencies have been achieved and considerably higher output is obtained from Nd:YVO_4 than from Nd:YAG [8]. Considering Q-switched operation, the high gain in combination with a short fluorescence lifetime produces relatively short Q-switch pulses compared to Nd:YAG and Nd:YLF. Pulsewidth in repetitively Q-switched systems is typically around 10 ns.

Longitudinally diode-pumped Nd:YVO_4 are commercially available; for fast marking application, Nd:YVO_4 should be preferred to Nd:YAG thanks to the shorter photon cavity lifetime that allows higher pulse repetition frequencies.

3.3.1.3 Nd:$GdVO_4$

Nd:$GdVO_4$ has recently attracted considerable attention as a novel solid-state material. Nd:$GdVO_4$ has the same space group as Nd:YVO_4, which has proved to be an excellent laser material [10]. In comparison with the Nd:YVO_4 crystal, Nd:$GdVO_4$ has a even higher absorption coefficient [11]. In literature, many affirm that Nd:$GdVO_4$ has a higher stimulated emission cross-section than Nd:YVO_4 (see, e.g., [10] [11]), but recent studies show the opposite [6]. Anyway, the most attracting property of the Nd:$GdVO_4$ crystal is its excellent thermal conductivity which is about two times larger than that of the Nd:YVO_4. Therefore, the Nd:$GdVO_4$ seems more suitable for high-power systems. In literature, a maximum output power of 19.8 W has been obtained in an end-pumped configuration under a pump power of 39.5 W [10].

3.3.2 Methods for Optical Pumping

The pump source of a solid state laser emits radiation in a spectral region that falls within the absorption bands of the lasing medium. Electrical energy, either continuous or pulsed is supplied to the pump source and converted into optical radiation. A highly reflective enclosure, or an optical system, couples the radiation from the pump source to the laser material. The most efficient pump will produce maximum emission at wavelengths which excite fluorescence in the laser material, and produce minimal emission in all spectral regions outside of the useful absorption bands. Nowadays, flashlamps, cw arc lamps and laser diodes are used as source pump for solid state lasers. Lamps are the traditional method for optical pumping, they emits at different wavelengths and have low efficiency. In the majority of the modern systems, lamp pumping has been replaced by laser diode pumping, and will be therefore no further analyzed here.

Laser beams have been often used to pump other lasers since the early days of laser development [3], but it has become a very important pumping technique, however, since efficient and high-power diode lasers have been developed and made widely available. The emission from laser diodes is highly directional, therefore many arrangements are possible for transferring the pump radiation to the solid-state laser material. Since the output beams of laser diodes can be shaped and focused, a major consideration is the design of a pump geometry which maximizes the overlap of the pumped volume with the volume occupied by a low-order resonator mode. The optimization of the overlap is referred to as mode-matching.

Typically, two basic approaches have been followed in diode pumping of solid-state lasers, namely *end-pumped* and *side-pumped* configurations. In the end-pumped technique, pump radiation is introduced longitudinally into the active material, i.e. co-linear with the resonator axis. In the side-pumped configuration, which is similar in concept to flashlamp pumped lasers, the radiation from the bars enters the active material transverse to the optical axis of the laser radiation. End-pumping is the more efficient method for generating diffraction limited performance, as the pump radiation is spatially overlapped with the TEM_{00} lasing mode [8]. Matching the high

aspect ratio of the emitting area of diode bars to the intracavity mode size is a very challenging optical task and a number of beam shaping techniques have been developed. If the pump beam stays well within the volume of the fundamental transverse mode of the laser resonator, transverse single-mode operation with diffraction-limited beam quality is often possible, because higher-order modes then have too low gain to reach the laser threshold. Although less efficient, side pumping of laser rods and slabs is easily scaled and is therefore mainly employed for high-power systems. In side-pumping, the high aspect ratio of the emitting surface can be accomplished over a larger surface area which reduced thermally related problems.

We consider the two cases separately because the corresponding diode lasers and pump-transfer systems are somewhat different.

3.3.2.1 Transverse Pumping

In this configuration, the diode arrays are placed along the length of the laser rod and pump perpendicularly to the direction of propagation of the laser radiation. As more power is required, more diode arrays can be added along and around the laser rod. There are two approaches to couple the radiation emitted by the laser diodes to the rod. a) *Direct coupling*: from a design standpoint this is by far the most desirable approach. However this arrangement does not allow for much flexibility in shaping the pump radiation inside the laser rod. b) *Intervening optics between source and absorber*: in this case, the pump distribution can be peaked at the center of the rod allowing for a better match with the resonator modes. Optical coupling can be achieved by using imaging optics such as lenses or elliptical and parabolic mirrors, or by non-imaging optics such as reflective or refractive flux concentrators.

Whether or not to use intervening optics between the arrays and the laser rod depends mainly on the desired beam diameter and optical density of the active medium. Generally speaking, oscillator pump heads usually employ optical elements in order to concentrate the pump radiation in the center for efficient extractions at the TEM_{00} mode, whereas large amplifier rods are direct pumped.

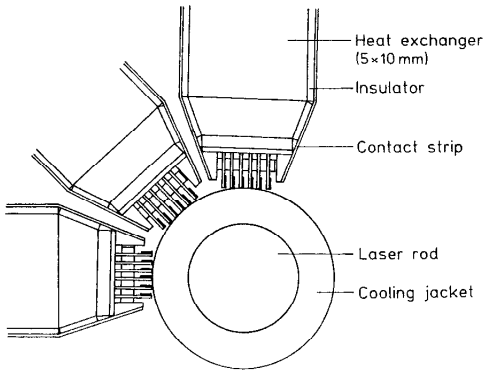

Figure 3.3: Example of a possible configuration for transverse pumping: stacked diode array bars around a laser rod

3.3.2.2 Longitudinal Pumping

The focused end-pumping configuration, if properly designed to provide matching of the pump light distribution and resonator mode, is the most efficient pump-radiation transfer scheme. Since the pump beam from the diode array is collinear with the optical resonator, the overlap between the pumped volume and the TEM_{00} mode can be very high. Practical realization of these advantages depends upon the possibility of reshaping a strongly astigmatic diode-laser beam into a generally small (100 μm-1 mm diameter) beam with possibly circular symmetry. The most common techniques of transferring and reformatting radiation from a single bar or stack of bars to an end-pumped laser crystal includes imaging optics (i.e., by the use of lenses and anamorphic optical systems), fiber optic coupling and nonimaging concentration (e.g., by the use of lens ducts).

The solution of a fiber-optic bundle to deliver the diode output to the laser crystal has a number of advantages: the beam at the fiber output has a circular distribution, and the ability to remove heat from the diode remote from the optical components of the laser is an attractive feature. Also, the pump source can be easily replaced without disturbing the alignment of the laser. A possible set-up for a double end-pumped configuration is shown in figure 3.4.

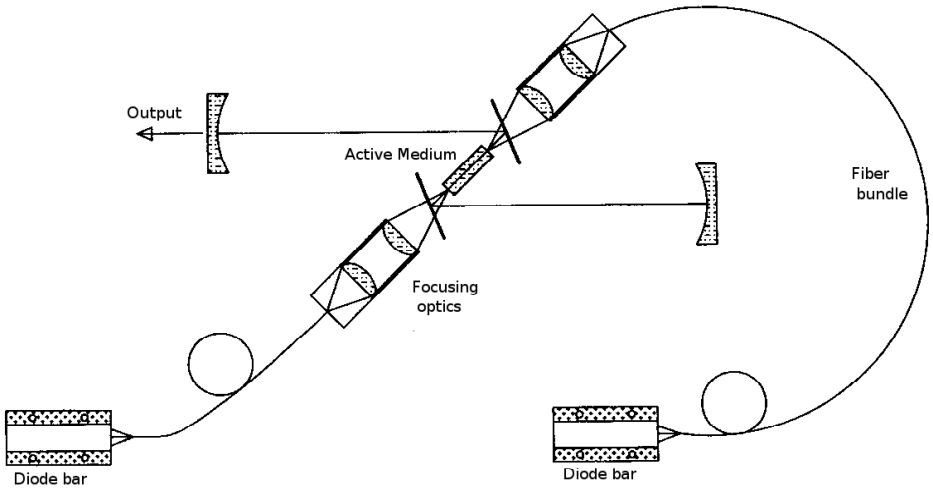

Figure 3.4: Example of a possible cavity configuration for fiber double end-pumped solid-state laser

3.3.2.3 Diode Lasers

Diode or semiconductor lasers are briefly described here because of their importance as pumps for solid-state lasers.

In diode lasers, the active medium is based on a combination of the elements in the third group of the Periodic Table (such as Al, Ga, In) and the fifth group (such as N, P, As, Pb) hence referred as *III-V compounds*. Examples include GaAs, as well as some ternary (e.g., AlGaAs, InGaAs) and quaternary (e.g., InGaAsP) alloys. The cw laser emission wavelength of these III-V compounds generally ranges from 630-1600 nm, but recently semiconductor lasers providing emission in the blue region ($\sim$ 410 nm) have been developed. Neodymium doped crystals have a peak of absorption at 808 nm, wavelength emitted by AlGaAs compounds. Although diode lasers are the most efficient lasers available ($\eta \sim 60$ %) [3], the output power of a single device cannot exceed a few hundred of milliwatts. In order to reach higher powers, several diodes are lined up in stacks (see fig. 3.5). Thanks to this set-up, very high power can be reached in a very small dimension, e.g., there exist 6 kW diode laser slightly bigger than a shoe box. In the output power range suitable for solid-state laser pumping, this stacks are not bigger than a cigarette pack. An important limitation for this technology is the

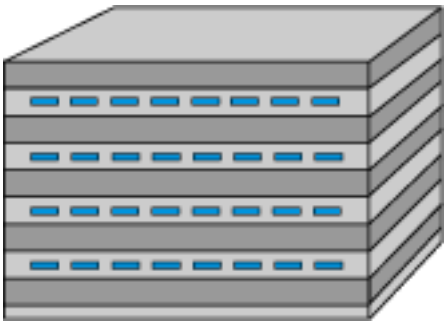

Figure 3.5: Schematic structure of a laser diode stack. The emitters are shown in blue, and the microchannel coolers in dark gray.

device lifetime, shorter than single emitters diodes (10-20 respect to 40-80 thousand hours).

3.4 Developed Source

In this work, a solid-state laser source will be analyzed and developed. The applications target exclude the use of a CO_2 source, while fiber lasers are not taken into account due to the device high cost and their maximum attainable irradiance (see section 3.2). The solid-state source will be of course diode pumped. Longitudinal pumping will be preferred over a transverse set-up for several reasons:

1. **Shorter cavity** allows shorter light pulses with higher peak powers. In fact, the pulse width is proportional to the cavity photon decay time, which in turn is proportional to the cavity length. According to Svelto [3]

$$\tau_c = -\frac{2L}{c\ln[R_1 R_2(1-T_i)^2]} \tag{3.1}$$

where L is the cavity length, R_1 and R_2 the mirrors reflectivity and T_i is the cavity internal loss per pass. The energy stored in the crystal is therefore released in a shorter time, giving higher peak powers.

2. **Higher Stability**. A shorter cavity results also in a higher mechanical stability because the cavity misalignment sensitivity is proportional to cavity length. See section 4.3.3 and equations (4.46) for details.

3. **Higher Optical Efficiency**. The pump light is mostly overlapped to the laser mode, on the contrary of a side-pump configuration where the whole crystal is enlighten. Therefore, the optical-to-optical efficiency in an end-pump configuration can reach 50%, while in a side-pump configuration it stands around 25%, giving twice the brightness with equal pump power.

4. **Nd:YVO_4 and Nd:$GdVO_4$**. The end-pump configurations allows an efficient use of short crystals such as Nd:YVO_4 and Nd:$GdVO_4$, which show better performances than Nd:YAG at high pulse repetitions frequencies, therefore being more suitable in fast marking applications.

The work will be mainly focused on Nd:YVO_4 as active media, since it is known to be an effective solution, already adopted by many other manufacturers. Experiments on Nd:$GdVO_4$ will also be performed in order to test the crystal promising physical properties. A 40 W diode laser will be used as pump source. The light will be delivered to the crystal via an optical fiber.

Chapter 4

Theoretical Analysis

In the last 20 years, a great effort has been produced with the purpose of scaling diode end-pumped lasers to high powers and much of this effort has been published and is available to the scientific community. Based on those works, in this chapter, the behavior of an end-pumped solid-state laser has been analyzed from a theoretical point of view, with the aim to develop tools useful in designing the laser source. In section 4.1 the properties of few gain media have been discussed. In section 4.2, a method to find the best coupling parameters has been found. Finally, in section 4.3, tools for a correct design of the resonator are proposed.

4.1 Active Medium

The choice between different active media will be limited to Nd:YVO_4 and Nd:$GdVO_4$, whose main properties has been described in section 3.3.1. Several advantages with respect to the traditionally used Nd:YAG crystals include a higher gain cross section, lower threshold, a wider absorption bandwidth, and polarized output. For example, the pump absorption bandwidth of Nd:YVO_4 crystals is 2.4-6.3 times that of Nd:YAG crystals [12]. The wider absorption bandwidth means that the laser output power is less sensitive to drift of the diode pump wavelength due to temperature or aging effects. In addition, Nd:YVO_4 crystals are uniaxial and they can produce only polarized laser output, thus avoiding undesirable birefringent effects.

Even though vanadate laser host materials have several advantages over Nd:YAG crystals in the design of diode-pumped lasers, their thermal conductivity is lower than that of Nd:YAG crystals, and a large amount of thermal energy converted from absorbed pump power is accumulated near the pump region. Theoretical and experimental studies show that the maximum laser output power for end-pumped solid-state lasers is limited by thermal fracture of laser crystals. Tsunekane et al. [13] reported that the maximum pump power limited by thermal fracture is approximately 13.5 W for a conventional 1.1 at. % Nd:YVO_4 crystal pumped from a single end. On the other hand, Tidwell et al. [14] estimated that the fracture-limited pump power for Nd:YAG crystals is around 50-70 W. The lower thermal conductivity is one of the reasons why the fracture-limited pump power for Nd:YVO_4 crystals is significantly lower than that for Nd:YAG crystals. In addition to thermal conductivity, the fracture-limited pump power for an end-pumped solid-state laser strongly depends on the absorption coefficient. The absorption coefficient of a 1.0 at. % Nd:YVO_4 crystal is five times that of a Nd:YAG crystal with the same dopant concentration at a pump wavelength of 808 nm. A high absorption coefficient makes it easy to obtain single-longitudinal-mode operation by using a short monolithic cavity [15]. Furthermore, a high absorption coefficient can lead to a high slope efficiency for the TEM_{00} mode. Nevertheless, a high absorption coefficient results in a large temperature gradient and, consequently, a large amount of stress produced at the pump end of the crystal. Tidwell et al. [14] and Cousins [16] have developed a model to analyze the scaling limits of diode-end-pumped Nd:YAG lasers imposed by thermal fracture. However, the influence of the absorption coefficient on the fracture-limited output power was never considered in their investigations. Pump absorption decreases linearly with dopant concentration; therefore, lowering the concentration for Nd:YVO_4 crystals extends the fracture-limited pump power, and there is a range in which Nd:YVO_4 crystals can still keep the pump absorption coefficients larger than those for Nd:YAG crystals. Therefore, it is of practical interest to determine the optimum dopant concentration for Nd:YVO_4 crystals in scaling to higher power in an end-pumped geometry.

Chen [12] showed that lowering the dopant concentration linearly extends

the fracture-limited pump power and found that the maximum output power in a 0.5 at. % Nd:YVO_4 crystal is 15.6 W from a 5 mm long crystal. He also predicted that a single Nd:YVO_4 crystal with 0.25 at. % dopant concentration can produce TEM_{00} mode output power higher than 20 W before thermal fracture occurs.

4.2 Pumping System

Laser diode-pumped solid-state lasers can offer high efficiency, compactness, and reliability, especially in an end-pumping configuration. A high efficiency is obtained with spatial matching between the pump beam and the laser cavity mode. In scaling end-pumped lasers to higher power, the fiber-coupled laser-diodes with circular beam profiles are often used as pump sources due to the fact that the high power diode lasers are very asymmetric in their emitting aperture dimensions. In addition, fiber delivery of the pump power allows to keep the laser resonator apart from the pump source, so that the laser resonator can be isolated from disturbances of the pump sources. Moreover, this set-up allows an easy replacement of the pump diodes and offers the possibility to build two independent cooling systems for the pump diodes and the laser cavity. However, pump-beam quality should be taken into account in the design of the fiber-coupled laser-diode end-pumped lasers. Mode size optimization in diode-end-pumped lasers has been investigated by several authors. We here rely on the works by Chen et al. [17] and Hajiesmaeilbaigi et al. [18] to analytically find the best coupling system for mode size optimization. It is found that the optimum pump and laser mode sizes are considerably affected by the pump beam quality.

According to Laporta and Brussard [19], on the basis of the space-dependent rate equation analysis, threshold pump power P_{th} and slope efficiency S_{e} are given by the following equations:

$$P_{\mathrm{th}} = \frac{\gamma I_{\mathrm{sat}}}{\eta_{\mathrm{p}} L} V_{\mathrm{eff}} \tag{4.1}$$

$$S_{\mathrm{e}} = \frac{T}{2\gamma} \eta_{\mathrm{p}} \eta_{\mathrm{o}} \tag{4.2}$$

where γ is the total logarithmic loss per pass, I_{sat} is the saturation intensity, L is the length of the active medium, T is the power transmission of the output coupler, and $\eta_{\mathrm{p}} = \eta_{\mathrm{t}}\eta_{\mathrm{a}}(\nu_{\mathrm{t}}/\nu_{\mathrm{p}})$ where ν_{t} is the optical transfer efficiency, η_{a} is the absorption efficiency and ν_{p} and ν_{l} are pump and laser frequencies, respectively. The effective mode volume V_{eff} and the overlapping efficiency η_{o} are given by the overlap integrals as

$$V_{\mathrm{eff}} = \left(\iiint S_{\mathrm{l}}(x,y,z) r_{\mathrm{p}}(x,y,z) \mathrm{d}\nu \right)^{-1} \tag{4.3}$$

$$\eta_{\mathrm{o}} = \frac{\left(\iiint S_{\mathrm{l}}(x,y,z) r_{\mathrm{p}}(x,y,z) \mathrm{d}\nu \right)^2}{\iiint S_{\mathrm{l}}^2(x,y,z) r_{\mathrm{p}}(x,y,z) \mathrm{d}\nu} \tag{4.4}$$

where $S_{\mathrm{l}}(x,y,z)$ is the normalized cavity mode intensity distribution and $r_{\mathrm{p}}(x,y,z)$ is the normalized pump intensity distribution in the active medium. Considering a single transverse mode TEM_{00}, $S_{\mathrm{l}}(x,y,z)$ can be given by

$$S_{\mathrm{l}}(x,y,z) = \frac{2}{\pi w_{\mathrm{l}}^2(z) L} \exp\left(-2\frac{x^2+y^2}{w_{\mathrm{l}}^2(z)} \right) \tag{4.5}$$

and

$$w_{\mathrm{l}}(z) = w_0 \sqrt{1 + (z\lambda_{\mathrm{l}}/\pi w_0^2)^2} \approx w_{\mathrm{c}} \tag{4.6}$$

Here w_{c} is the laser beam radius in the crystal considered to be constant (see section 4.3.3), λ_{l} is the laser wavelength and the point z = 0 is taken to be at the incident surface of the active medium.

For a fiber-coupled pump beam, $r_{\mathrm{p}}(x,y,z)$ can be approximately described as a "top-hat" distribution

$$r_{\mathrm{p}}(x,y,z) = \frac{\alpha e^{-\alpha z}}{\pi w_{\mathrm{p}}^2(z)[1-e^{-\alpha L}]} \Theta(w_{\mathrm{p}}^2(z) - x^2 - y^2) \tag{4.7}$$

where α is the absorption coefficient at the pump wavelength, $w_{\mathrm{p}}(z)$ is the pump beam in the active medium, and $\Theta()$ is the Heaviside step function. On the basis of paraxial approximation, $w_{\mathrm{p}}(z)$ may be given by [19]

$$w_{\mathrm{p}}(z) = w_{\mathrm{po}} + \theta_{\mathrm{p}}|z - z_{\mathrm{o}}| \tag{4.8}$$

where w_{po} is the pump radius at the waist, θ_{p} and z_{o} are the far-field half-angle and pump waist position in the active medium, respectively. The brightness theorem gives a relationship for a given beam between any beam waist w, its associated far-field angle θ, and the refractive index n of the kind

$$n\theta w = C \geq \lambda/\pi \tag{4.9}$$

where λ is the beam wavelength and C expresses the beam quality. In terms of M^2 parameter, $C = M^2\lambda/\pi$ [20]. For a fiber-coupled laser diode the value of C is easily calculated from its core radius r_{c} and divergence angle θ. Therefore, the relationship between w_{po} and θ_{p} is given by

$$\theta_{\mathrm{p}} = \frac{C}{n w_{\mathrm{po}}} \tag{4.10}$$

With Eqs. (4.1) - (4.10), both P_{th} and S_{e} can be written in terms of the match function F:

$$F\left(C/n, \alpha, L, z_{\mathrm{o}}, w_{\mathrm{c}}, w_{\mathrm{po}}\right) = \frac{1}{1-\exp(-\alpha L)} \times \int_0^L \frac{\alpha w_{\mathrm{c}}^2 \exp(-\alpha z)}{w_{\mathrm{c}}^2 + \left[w_{\mathrm{po}} + [C/(n w_{\mathrm{po}})]|z - z_{\mathrm{o}}|\right]^2} \mathrm{d}z \tag{4.11}$$

which describes the spatial overlap of the pump beam and resonator mode. The maximum value of the match function leads to the lowest threshold and the highest slope efficiency [17]. By introducing the variables $\xi = \alpha z$, $d = \alpha L$ and the parameter $\beta = C/n\alpha$, equation (4.11) can be simplified as

$$F(\beta, d, \xi_{\mathrm{o}}, w_{\mathrm{c}}, w_{\mathrm{po}}) = \frac{1}{1-e^{-d}} \times \int_0^d \frac{w_{\mathrm{c}}^2 e^{-\xi}}{w_{\mathrm{c}}^2 + \left[w_{\mathrm{po}} + (\beta/w_{\mathrm{po}})|\xi - \xi_{\mathrm{o}}|\right]^2} \mathrm{d}\xi \tag{4.12}$$

Eq. (4.12) states that the match function depends on the pump-beam quality and properties of the active medium. In terms of the match function,

$P_{\rm th}$ and $S_{\rm e}$ are given by [18]

$$P_{\rm th}(\beta, d, \xi_{\rm o}, w_{\rm c}, w_{\rm po}) = \frac{\pi\gamma I_{\rm sat} w_{\rm c}^2}{2\eta_{\rm p}} \frac{1}{F(\beta, d, \xi_{\rm o}, w_{\rm c}, w_{\rm po})} \tag{4.13}$$

and

$$S_{\rm e}(\beta, d, \xi_{\rm o}, w_{\rm c}, w_{\rm po}) = \frac{T\eta_{\rm p}}{2\gamma} \frac{[F(\beta, d, \xi_{\rm o}, w_{\rm c}, w_{\rm po})]^2}{F(\beta, d, \xi_{\rm o}, w_{\rm c}/\sqrt{2}, w_{\rm po})} \tag{4.14}$$

Then, the output power can be expressed as

$$P_{\rm out}(P_{\rm in}, \beta, d, \xi_{\rm o}, w_{\rm c}, w_{\rm po}) = S_{\rm e}(\beta, d, \xi_{\rm o}, w_{\rm c}, w_{\rm po}) \times [P_{\rm in} - P_{\rm th}(\beta, d, \xi_{\rm o}, w_{\rm c}, w_{\rm po})] \tag{4.15}$$

where $P_{\rm in}$ is the input power. Although there is no analytical solution for the match function as it is, a suitable approximation can be applied. Replacing $w_{\rm p}(z)$ in eq. (4.7) by the average pump size $\bar{w}_{\rm p}$, eq. (4.15) can be analytically expressed as

$$P_{\rm out}(P_{\rm in}, a, \bar{w}_{\rm p}) = \frac{T\eta_{\rm p}}{2\gamma} \frac{a(a+2)}{(a+1)^2} \left[P_{\rm in} - \frac{\pi\gamma I_{\rm sat} \bar{w}_{\rm p}^2}{2\eta_{\rm p}} (a+1) \right] \tag{4.16}$$

where $a = (w_{\rm c}/\bar{w}_{\rm p})^2$.

Laporta and Brussard [19] have used eq. (4.16) to derive the optimum value of a for the maximum output with the assumption that $w_{\rm p}(z)$ is a constant. They demonstrated how the lowest threshold and the highest slope efficiency are obtained for $\bar{w}_{\rm p} \to 0$. It is evident that the minimum value of $\bar{w}_{\rm p}$ is limited by pump-beam quality, properties of the active medium and focus position. It is therefore of great practical interest to determine the minimum value of $\bar{w}_{\rm p}$ for a given pump-beam quality and properties of the active medium.

The average pump size for a fiber-coupled laser diode can be written as [18]

$$\bar{w}_{\rm p}(\beta, w_{\rm po}, \xi_{\rm o}, d) = \frac{\int_0^d [w_{\rm po} + (\beta/w_{\rm po})|\xi - \xi_{\rm o}|] e^{-\xi} d\xi}{\int_0^d e^{-\xi} {\rm d}\xi} \tag{4.17}$$

The weighting function $e^{-\xi}$ in eq. (4.17) originates from the absorption effect. Carrying out the integration of d, after some algebra, it is obtained:

$$\bar{w}_{\mathrm{p}}(\beta, w_{\mathrm{po}}, \xi_{\mathrm{o}}, d) = w_{\mathrm{po}} + \frac{\beta}{w_{\mathrm{po}}} \times \left[(\xi_{\mathrm{o}} - 1) \coth\left(\frac{d}{2}\right) + \frac{2e^{-\xi_{\mathrm{o}}} - de^{-d}}{1 - e^{-d}} \right] \quad (4.18)$$

At a fixed β and w_{po}, the optimum focal position $z_{\mathrm{o,opt}}$ for minimizing $\bar{w}_{\mathrm{p}}$ can be obtained by imposing the condition

$$\left. \frac{\partial \bar{w}_{\mathrm{p}}(\beta, w_{\mathrm{po}}, \xi_{\mathrm{o}}, d)}{\partial \xi_{\mathrm{o}}} \right|_{\xi_{\mathrm{o}} = \alpha z_{\mathrm{o,opt}}} = 0 \quad (4.19)$$

This equation yields the solution

$$z_{\mathrm{o,opt}} = \frac{1}{\alpha} \ln\left(\frac{2}{1 + e^{-d}}\right) \quad (4.20)$$

The minimum average pump spot size is derived by substituting equation (4.20) into (4.18) and differentiating with respect to w_{po}. The positive roots gives for the optimum value of w_{po} at a fixed β

$$w_{\mathrm{po,opt}} = \left\{ \beta \left[\left(\ln\left(\frac{2}{1 + e^{-d}}\right) - 1 \right) \coth\left(\frac{d}{2}\right) + \frac{1 + e^{-d} - de^{-d}}{1 - e^{-d}} \right] \right\}^{1/2} = [\beta A(d)]^{1/2} \quad (4.21)$$

where

$$A(d) = \left[\left(\ln\left(\frac{2}{1 + e^{-d}}\right) - 1 \right) \coth\left(\frac{d}{2}\right) + \frac{1 + e^{-d} - de^{-d}}{1 - e^{-d}} \right] \quad (4.22)$$

Then from eq. (4.10), the optimum far-field half angle is given by

$$\theta_{\mathrm{po,opt}} = \frac{1}{[\beta A(d)]^{1/2}} \times \frac{C}{n} = \left[\frac{C\alpha}{nA(d)} \right]^{1/2} \quad (4.23)$$

Equations (4.20), (4.21) and (4.23) are a useful guideline to design the optical coupling system. Note that both $w_{\mathrm{po,opt}}$ and $\theta_{\mathrm{po,opt}}$ have been related to the pump beam quality and properties of the active medium. So, for example, if we consider a 10 mm long crystal with an absorption coefficient

$\alpha = 0.4$ mm^{-1} and a pump light with $M^2 = 60$, according to the previous equations, the optimum waist position is $z_{\mathrm{o,opt}} = 1,69$ mm, the pump waist radius is $w_{\mathrm{po,opt}} = 0,11$ mm and the far-field angle $\theta_{\mathrm{po,opt}} = 0.07$ rad.

4.3 Resonator Design

The main problem in designing a resonant cavity for a solid-state laser consists in the laser mode perturbations introduced by active medium heating. Possible consequences of high temperature in the active medium are thermal lensing and birefringence. Flattening and non-Gaussian output intensity profiles have also been reported [8].

Optical pumping leads to a radial temperature gradient in the laser rod. As a result, in cw and high average power systems, the rod is acting like a positive thick lens of an effective focal length *f*, which is inversely proportional to the pump power. It is convenient to represent a resonator with an internal lenslike medium as a resonator with an internal thin lens. The equivalent cavity is shorter than the real one, see fig. 4.1. The distance h of the lens principal planes from the rod ends is given by [21]

$$h = \frac{L}{2n} \tag{4.24}$$

4.3.1 Thermal Lensing

Particularly in high-power lasers, the heating of the gain medium often causes a significant thermal lens through the following mechanisms:

- The gain medium is hotter on the beam axis, compared with the outer regions, typically causing some transverse gradient of the refractive index ($\rightarrow$ thermooptic effect, quantified with the coefficient $\mathrm{d}n/\mathrm{d}T$).

- Further index changes can be caused by thermally induced mechanical stress ($\rightarrow$ photoelastic effect, quantified with photoelastic coefficients ρ_{ij} and the thermal expansion coefficient α_{T}).

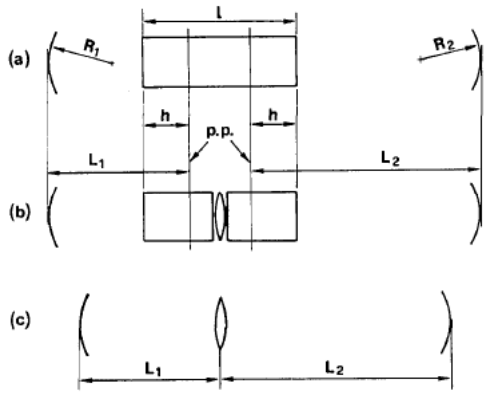

Figure 4.1: Equivalent resonators with (a) a lenslike rod; (b) a thin lens between two pieces of homogeneous material [exactly equivalent to (a) outside the rod and approximately inside]; (c) a thin lens [equivalent to (a) and (b) outside the rod]. The spot sizes on the lenses are the same in (b) and in (c), and approximately equal to that in the middle of the rod in (a); p.p. = principal plane. [21]

- Mechanical stress can also lead to bulging of the end faces of the gain medium, so that these also cause lensing. This effect can be important for short laser crystals.

Depending on the situation, these effects might have different relative strength and even sign. In many cases, the first mentioned effect (temperature dependence of the refractive index) is most important. A widely used formula, firstly derived by Innocenzi et al. [22] and afterwards modified by Cousins [16] and others, for theoretical calculation of thermal lens focal length is

$$f_{\mathrm{T}} = \frac{2\pi K_{\mathrm{c}}}{A_0} \frac{\bar{w}_{\mathrm{p}}^2}{\xi P_{\mathrm{abs}}} \tag{4.25}$$

where K_{c} is the thermal conductivity, P_{abs} is the absorbed pump power and ξ is the fractional thermal loading, i.e., the fraction of pump power that is transformed into heat. The parameter A_0 is related to the characteristics of the crystal and is derived from the optical path difference (OPD) theory (see, e.g, [23, 20]):

$$A_0 = \frac{\partial n}{\partial T} + (n-1)(1+\nu)\alpha_{\mathrm{T}} + 2C_{\mathrm{r}} n^3 \alpha_{\mathrm{T}} \tag{4.26}$$

where $\frac{\partial n}{\partial T}$ is the thermal optical coefficient, ν is Poisson's ratio and C_r is the photoelastic coefficient. The first term results from thermal dispersion, the second term is caused by the axial strain distribution and the third term represents the strain-induced birefringence. Note also that the factor $(n-1)$ has to be replaced by n in the case of end-pumped resonators with a high reflectivity coating at lasing wavelength on one end surface of the rod [20]. According to Fan et al. [23], the actual thermal lens focal length is larger than that calculated by eq. (4.25). This is due to a non-suitable approximation in OPD theory that gives precise enough values only in the case of $w_\mathrm{c}^2 \ll \bar{w}_\mathrm{p}^2$. In fact, the pump radius is usually about the same as the laser mode radius, and eq. (4.25) needs to be corrected as follows:

$$f_\mathrm{T} = \frac{2\pi K_\mathrm{c}}{A_0} \frac{\bar{w}_\mathrm{p}^2}{\xi P_\mathrm{abs}} r_f \tag{4.27}$$

where the correction factor r_f is a function of $w_\mathrm{c}/\bar{w}_\mathrm{p}$ and needs to be estimated experimentally. It was measured by Fan et al. [23] that in the usual condition of $w_\mathrm{c} \approx \bar{w}_\mathrm{p}$ r_f is higher than 1.5, i.e., there is an error higher than 50% in eq. (4.25).

4.3.2 Stability Analysis

The stability condition for a resonator is easily found with the use of geometric optics as shown by Svelto [3]. In paraxial approximation, the round-trip of a light ray into a resonator can be described by the $ABCD$ matrix of the resonator. If, after an infinite number of round-trips, the light ray is still inside the resonator, than the resonator is said to be stable. Mathematically, this can be expressed as follows: the matrix

$$\begin{vmatrix} A & B \\ C & D \end{vmatrix}^n$$

must not diverge as n increase. The condition is satisfied if and only if:

$$-1 < \left(\frac{A+D}{2} \right) < 1 \tag{4.28}$$

To simplify the calculations it is convenient to transform our resonator in fig. 4.1 into an equivalent resonator where each spherical mirror is replaced by a combination of a plane mirror and a thin lens of focal length equal to the mirror radius [3]. It is hence possible to express the round-trip matrix as the product of the single-pass $A_1B_1C_1D_1$ and single-pass backward matrices (obtained from the $A_1B_1C_1D_1$ matrix by interchanging elements A_1 and D_1 [3]). The round-trip matrix is therefore given by:

$$\begin{vmatrix} A & B \\ C & D \end{vmatrix} = \begin{vmatrix} D_1 & B_1 \\ C_1 & A_1 \end{vmatrix} \begin{vmatrix} A_1 & B_1 \\ C_1 & D_1 \end{vmatrix} = \begin{vmatrix} 2A_1D_1 - 1 & 2B_1D_1 \\ 2A_1C_1 & 2A_1D_1 - 1 \end{vmatrix} \tag{4.29}$$

Now, from eqs. (4.28) and (4.29), in terms of one-way matrix elements, the resonator stability condition can be simply written as

$$0 \leq A_1D_1 \leq 1 \tag{4.30}$$

So, in the case of an active resonator with spherical mirrors the single-pass matrix can be calculated as follows:

$$\begin{aligned} \begin{vmatrix} A_1 & B_1 \\ C_1 & D_1 \end{vmatrix} &= \begin{vmatrix} 1 & 0 \\ -\frac{1}{R_2} & 1 \end{vmatrix} \begin{vmatrix} 1 & L_2 \\ 0 & 1 \end{vmatrix} \begin{vmatrix} 1 & 0 \\ -\frac{1}{f} & 1 \end{vmatrix} \begin{vmatrix} 1 & L_1 \\ 0 & 1 \end{vmatrix} \begin{vmatrix} 1 & 0 \\ -\frac{1}{R_1} & 1 \end{vmatrix} = \\ &= \begin{vmatrix} 1 - \frac{L_2}{f} - \frac{L_0}{R_1} & L_0 \\ \frac{L_0}{R_1R_2} - \frac{1}{R_1} - \frac{1}{R_2} - \frac{1}{f}\left(1 - \frac{L_1}{R_1} - \frac{L_2}{R_2}\right) & 1 - \frac{L_1}{f} - \frac{L_0}{R_2} \end{vmatrix} \end{aligned} \tag{4.31}$$

where L_1 and L_2 are the distances between the mirrors and the lens (or the principal planes of the crystal), R_1 and R_2 are the radii of curvature of the mirrors (positive if concave) and $L_0 = L_1 + L_2 - (L_1L_2/f)$.
By introducing the dimensionless parameters g_1 and g_2 defined as :

$$g_1 = 1 - \frac{L_2}{f} - \frac{L_0}{R_1}; \qquad g_2 = 1 - \frac{L_1}{f} - \frac{L_0}{R_2} \tag{4.32}$$

it is possible to plot a stability diagram for the resonator. Stable configurations for the resonator are those enclosed by a branch of the hyperbola $g_1g_2 = 1$ and the coordinate axes, see fig. 4.2. It is evident how the resonator stability is function of the thermal lens focal length, which, in turns, varies

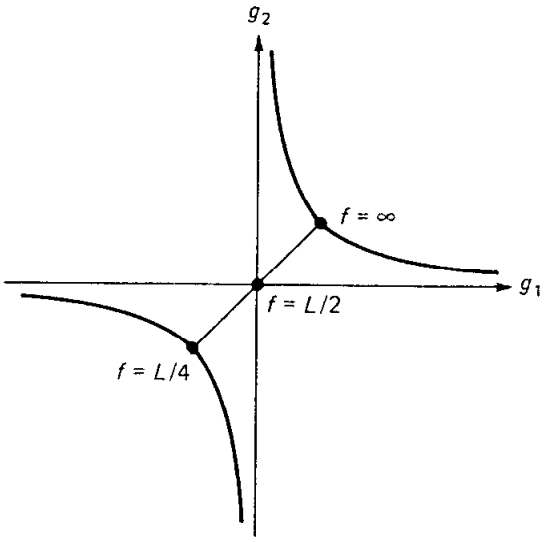

Figure 4.2: Stability diagram of a resonator with plane-parallel mirrors containing a thin positive lens [8]

with pump power according to eq. (4.27). Resonator length and mirrors radii must therefore be chosen to make the resonator stable at the desired working regime, and possibly in a wide range around it.

4.3.3 Misalignment Stability

An analysis of the misalignment stability is very important for a laser source which is going to be used in a productive environment. The manufacturer has to guarantee the performances of its product when it will leave the test laboratories. It is therefore important to study the sensitivity of the product to external interferences, such as vibrations and mechanical perturbations. The analysis was firstly carried out by Magni [21] and here we will rely on his work.

Firstly, it is convenient to introduce three new variables

$$u_1 = L_1\left(1 - \frac{L_1}{R_1}\right), \qquad u_2 = L_2\left(1 - \frac{L_2}{R_2}\right), \tag{4.33}$$

$$x = \frac{1}{f} - \frac{1}{L_1} - \frac{1}{L_2} \tag{4.34}$$

in order to simplify the calculations. The parameters g_1, g_2 and L_0 are redefined as follows:

$$g_1 = -\frac{L_2}{L_1}(1 + xu_1), \qquad g_2 = -\frac{L_1}{L_2}(1 + xu_2), \tag{4.35}$$

$$L_0 = -L_1 L_2 x \tag{4.36}$$

Now, the resonator stability condition $0 \leq g_1 g_2 \leq 1$ can be rewritten as

$$0 \leq (1 + xu_1)(1 + xu_2) \leq 1 \tag{4.37}$$

Equations (4.35) also indicate that the points of the (g_1, g_2) plane related to a given resonator configuration describe, as the focal length (i.e., x) varies, a straight line, as shown in fig. 4.3. The intersection of this line with the axes and with the hyperbola $g_1 g_2 = 1$ gives the critical values of x corresponding to the edges of the stability regions. These are:

$$\frac{1}{f} = \begin{cases} \frac{1}{L_2} + \frac{1}{L_1 - R_1} & \text{for } g_1 = 0, \\ \frac{1}{L_1} + \frac{1}{L_2 - R_2} & \text{for } g_2 = 0, \\ \frac{1}{L_1} + \frac{1}{L_2} & \text{for } g_1 g_2 = 1, \\ \frac{1}{L_1 - R_1} + \frac{1}{L_2 - R_2} & \text{for } g_1 g_2 = 1. \end{cases} \tag{4.38}$$

Following Magni's notation, zone I is the region of stability characterized at one of the two edges by focal points of the mode on both mirrors. The other region, for which at one edge the beam size on both mirrors diverges, will be called zone II. More precisely, zone I is defined by: $|xu_1| < 1 \wedge |xu_2| < 1$ and zone II is defined as $|xu_1| > 1 \ \wedge | \ xu_2| > 1$.

In any resonator, the TEM_{00} mode spot size at one mirror can be expressed as a function of the resonator parameters [21]

$$w_1^2 = \frac{\lambda L_0}{\pi} \left(\frac{g_2}{g_1(1 - g_1 g_2)} \right)^{1/2} \qquad w_2^2 = \frac{\lambda L_0}{\pi} \left(\frac{g_1}{g_2(1 - g_1 g_2)} \right)^{1/2} \tag{4.39}$$

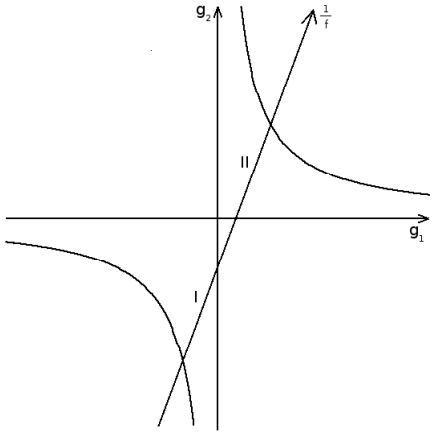

Figure 4.3: Stability diagram and stability zones (marked I and II). The point (g_1, g_2) representing the resonator moves linearly with the dioptric power $1/f$ on the lens along the straight line [21]

and the spot size w_0 at the beam waist is [3]

$$w_0^2 = \frac{\lambda L_0}{\pi}\left(\frac{g_1 g_2(1-g_1 g_2)}{g_1+g_2-2g_1 g_2)^2}\right)^{1/2} \tag{4.40}$$

The spot size w_c on the lens can be derived from equations (4.39) is given by:

$$w_c^2 = \frac{\lambda}{\pi}\frac{|2xu_1u_2+u_1+u_2|}{[(1-g_1g_2)g_1g_2]^{1/2}} \tag{4.41}$$

Since the spot size in the gain medium is directly responsible for the output power of the laser, it is suitable to maintain it as constant as possible under variations in input power and, consequently, in thermal focal length. The equation

$$\frac{\mathrm{d}w_c}{\mathrm{d}(1/f)} = \frac{\mathrm{d}w_c}{\mathrm{d}x} = 0 \tag{4.42}$$

has to be satisfied at the value of f corresponding to the working input power. On this condition, the resonator is considered dynamically stable. The stationary value w_{co} of the spot size on the lens, which is solution of

eq. (4.42) is simply given by

$$w_{\mathrm{co}}^2 = \frac{2\lambda}{\pi}\left|\Delta\frac{1}{f}\right|^{-1} \tag{4.43}$$

where $|\Delta(1/f)|$ is the width of the stability zones in terms of the dioptric power and is given by

$$\left|\Delta\frac{1}{f}\right| = \left|\Delta x\right| = \min\left(\left|\frac{1}{u_1}\right|, \left|\frac{1}{u_2}\right|\right) \tag{4.44}$$

It can be shown that the spot size w_{c} varies quite slowly in the middle of the stability zone and is, at most, 7% higher than w_{co}; thus, w_{co} can also be regarded as a stationary point for w_{c}.

With the help of w_{co}, two misalignment sensitivity factors for mirrors 1 and 2 can be defined as [21]

$$S_1 = \frac{d_1}{w_{\mathrm{co}}\alpha_1} \qquad S_2 = \frac{d_2}{w_{\mathrm{co}}\alpha_2} \tag{4.45}$$

where d_1 (or d_2) is the displacement of the mode axis on the lens caused by a tilting of mirror 1 (or 2), and α_1 (or α_2) is the rotation angle of mirror 1 (or 2). The misalignment sensitivity factors are related to the resonator parameters as follows:

$$S_1 = \frac{1}{w_{\mathrm{co}}}\frac{L_1}{u_1}\left(\frac{1}{u_1} + \frac{1}{u_2} + x\right)^{-1} \quad S_2 = \frac{1}{w_{\mathrm{co}}}\frac{L_2}{u_2}\left(\frac{1}{u_1} + \frac{1}{u_2} + x\right)^{-1} \tag{4.46}$$

An overall sensitivity is simply defined as

$$S = (S_1^2 + S_2^2)^{1/2} \tag{4.47}$$

According to Magni [21], as rule of the thumb, it may be assumed that $1/S$ is approximately the tilt angle for about a 10% increase in the losses. S is therefore an important parameter to estimate the tolerances on mirrors alignment and hence it is of fundamental importance when designing a reliable industrial laser.

Chapter 5

Source Design

In this chapter a laser source suitable for fast engraving operation is designed. Mandatory goals requested by SEI S.p.A. are:

- **High Efficiency.** In terms of energy conversion from the wall-plug to the laser output, high efficiency means that only a small amount of energy will be dispersed as heat. As a consequence, this will allow the design of a compact air-cooled solution instead of a standard, expensive and bulky water-cooled set-up.
- **Material Removal Capability at High Speed.** Speed is a major concern in every industrial application. Therefore the laser system shall be capable of emitting repeatable high peak pulses at high repetition frequencies (> 50 kHz).
- **Reliability.** Mandatory for every industrial machine, each single component of the laser system shall have a high MTBF (Mean Time Before Failure). Moreover, the performance of the system shall be as stable as possible in long term operation. The lifetime of the whole system should be higher than five years.

Other special demands were also:

- **Size.** The whole source, pump system included, must be as compact as possible, in order to have a clear advantage over other competitors in the market. In particular, the resonant cavity dimension should be smaller than 200 mm but bigger than 100 mm so to have room enough for easy fixing and replacement of internal components.

- **Output Power.** A market analysis showed that a source with an output power of at least 10 W in continuous wave would have a good success.
- **Beam Quality.** Beam quality is very important for fast engraving capability and precise processing. The goal is to have a beam with circular uniform shape, with a beam quality parameter $M^2 < 2$.
- **Cost.** Simple and low cost solutions are to be preferred whenever not strictly necessary, e.g. plane mirrors over curved mirrors, standard laser crystal over composite crystals, etc.
- **Industrial Product.** The making and the design of the system has to be simple, in order to guarantee a high productive process repeatability and reliability.

In section 5.1 a proper pumping system is evaluated. In section 5.2 a simple coupling optics is studied. In section 5.3 the laser cavity is analyzed in terms of stability and sensitivity. In section 5.4 the choice of a peculiar active medium is explained. Finally, in section 5.5 the main results are summarized.

5.1 Pumping System

The pumping device was chosen in order to have a long lifetime together with a good brightness. A single-emitters fiber-coupled diode satisfies this demands and it is also a very suitable component for an industrial device for three main reasons: (1) it allows an easy placement when designing the system and a quick re-placement in case of failure, with no need to re-align the optics (2) it has a very high lifetime (40 to 80 thousand hours - compared to actual technologies based on diode arrays, with lifetime around 10-20 thousand hours) (3) it adsorbs low current and allows a simple power supply design. The chosen device (see figure 5.1), emits at 808.1 nm. The device output power is up to 40 W, current-driven, with a slope efficiency of approximately 8.6 W/A. Measurements of the input/output performance has been carried out by the means of a thermal head with 250 W maximum measure power and an accuracy of $\pm 3\%$ (Ophir-Spiricon Inc, model FL250A) connected to an external display (Ophir-Spiricon Inc, model Laserstar). The

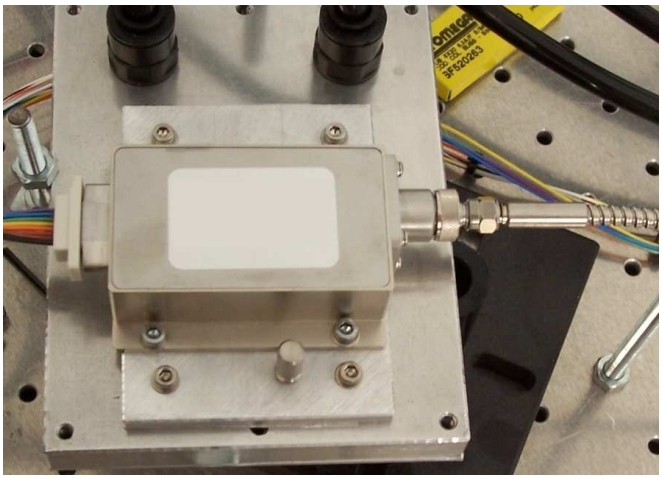

Figure 5.1: The laser diode fiber-coupled module used as pump source

measured input/output relation, plotted in fig. 5.2, shows a high linearity and confirms manufacturer's specifications.

The output power results to be stable at slightly different temperatures, around the optimum working temperature of 25 ℃. The manufacturer reports a wavelength shift of 0.28 nm per Celsius degree.

Pump light is coupled into an optic fiber with a 400 μm core diameter, 1.5 m in length and a measured numerical aperture $NA = 0.16$. Therefore, according to section 4.2, the pump beam quality expressed by the parameter C (see eq. (4.9)) is easily calculated from the fiber core radius r_c and divergence angle θ:

$$C = r_c \cdot \arcsin(NA) = 400/2\,\mu\text{m} \cdot \arcsin(0.16) = 0.032\,\text{mm} \tag{5.1}$$

that, in terms of the M^2 parameter, becomes

$$M^2 = C \cdot \pi/\lambda = 0.032\,\text{mm} \cdot \pi/\,808.1 \cdot 10^{-6}\,\text{mm} = 124.9 \tag{5.2}$$

As already discussed in chapter 4, pump quality is of fundamental importance in order to obtain a highly efficient and high quality output. It must be noted that the spot emitted from the provided fiber could not be consid-

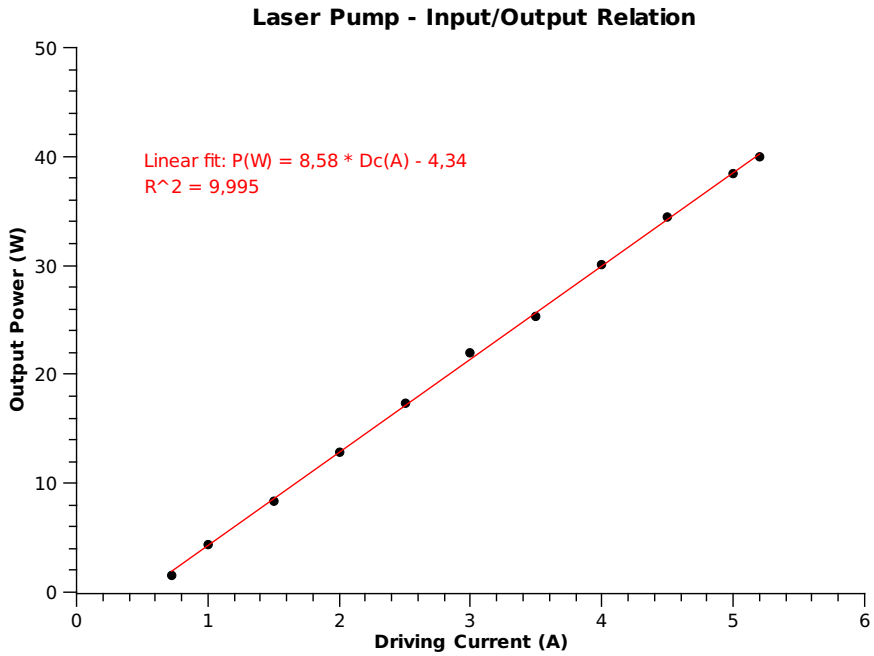

Figure 5.2: Laser diode pump input/output relation

ered as a top-hat distribution but was in fact very similar to a ring. This was more than evident by simply observing the beam a few centimeter out of the fiber. It is therefore expected that the output quality of the laser beam will be affected, in particular, higher order modes will be generated, leading to a high value of the M^2. Anyhow, this will allow to reach the crystal thermal fracture limit.

5.2 Coupling Optics

Pump light must be collected from the optic fiber and focused into the gain medium. The simplest way to achieve this is by means of a pair of lenses. Few calculations and the help of equations (4.21) and (4.23) allow to find the best solution. The beam diameter on the lenses depends on the focal length f_1 of the lens collecting the light from the fiber according to a simple geometrical relation:

$$D = 2f_1 \tan\left[\arcsin(NA)\right] \tag{5.3}$$

	D (mm)	w_{po} (mm)	θ_{p} (mrad)
Optimum		0.183	88.9
$f_1 = f_2$		0.198	82.2
$f_1 = 25.4, f_2 = 50.8$	8.23	0.396	41.1
$f_1 = 50.8, f_2 = 25.4$	16.47	0.099	164.4

Table 5.1: Lenses position influence on pump beam parameters. The theoretical optimum is shown, a solution that best approximate the optimum is proposed.

The waist of a laser beam going through a lens is given by [3]:

$$w_{\mathrm{po}} = 2M^2 \frac{\lambda f_2}{\pi D} = 2\,C\,\frac{f_2}{D} \tag{5.4}$$

The far-field angle in the crystal is derived from the definition of the beam quality parameter C according to eq. (4.10), repeated here:

$$\theta_{\mathrm{p}} = \frac{C}{n w_{\mathrm{po}}}$$

According to equations (4.21) and (4.23), the optimum pump waist and far-field angle can be derived by the physical parameters of the gain medium and the pump beam quality. The requested parameters for the active medium are: length $L = 10$ mm, refractive index at 808 nm $n = 1.9721$, absorbance $\alpha = 0.23$ mm^{-1} (see section 5.4 for further details). Numerical solutions to the previous equations are summarized in table 5.1

As it is evident form the table, the best set-up would consist in two lenses with identical focal length. Actually, several combinations were tested, with plano-convex glass lenses (BK7 - 25.4 mm diameter) with different focal lengths ($f_{\mathrm{a}} = 25.4$ mm, $f_{\mathrm{b}} = 50.8$ mm). It resulted that by using two identical lenses, it was possible to get the lowest lasing threshold and the best output quality at low pump powers (< 10 W). It was observed that by increasing the pump power, the beam quality rapidly decreased and maximum output powers were very low. This was due to thermal effects arising in the crystal, as it was evident from a qualitative analysis of the laser beam. On the other hand, by using two different lenses, in particular the combination of $f_1 = 25.4, f_2 = 50.8$, in spite of a higher lasing threshold and worse beam

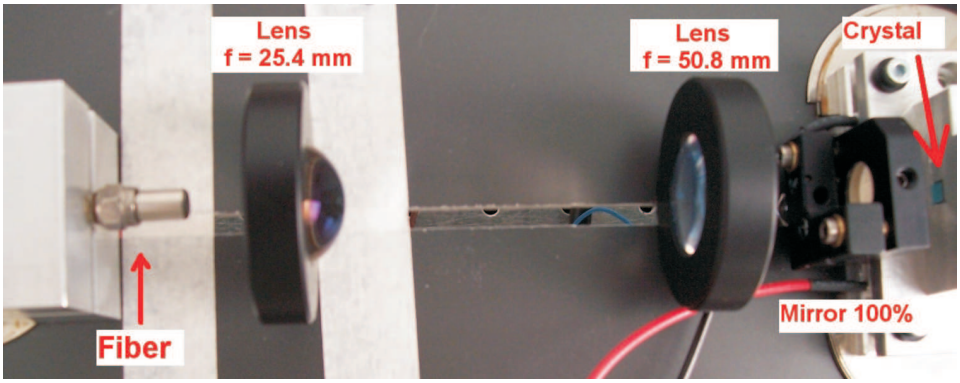

Figure 5.3: Coupling optic set-up

quality, much higher output powers could be reached. So, of the possible set-ups, the one that gives bigger waist and smaller divergence was chosen, in order to reduce the irradiance in the laser crystal, i.e. to reduce heating and thermal effects. Finally, the working parameters for the pump beam results $w_{\mathrm{po}} = 0.396$ mm and $\theta_{\mathrm{p}} = 41.1$ mrad. The convex sides of the lenses are faced in order to minimize optical aberrations. The final set-up is shown in figure 5.3. Measurements were carried out to evaluate coupling losses. It was found that the pump power after the two lenses is reduced by 3.3%.

5.3 Laser Cavity

The laser cavity is required to be linear and to have a dimension between 100 and 200 mm. The laser crystal is placed close to the 100% reflectivity mirror, in order to be at the proper distance from the coupling lens. The AO Q-switch is placed a few centimeters far, as shown in fig. 5.4(a) and fig. 5.5.

A resonant cavity with plane-parallel mirrors was chosen for the sake of simplicity in mirrors alignment and for low cost of the components. Such a resonator becomes dynamically stable when the crystal warming make the active medium behave as a lens. For a simple mathematical treatment, the resonator in fig. 5.4(a) can be transformed into the equivalent resonator in

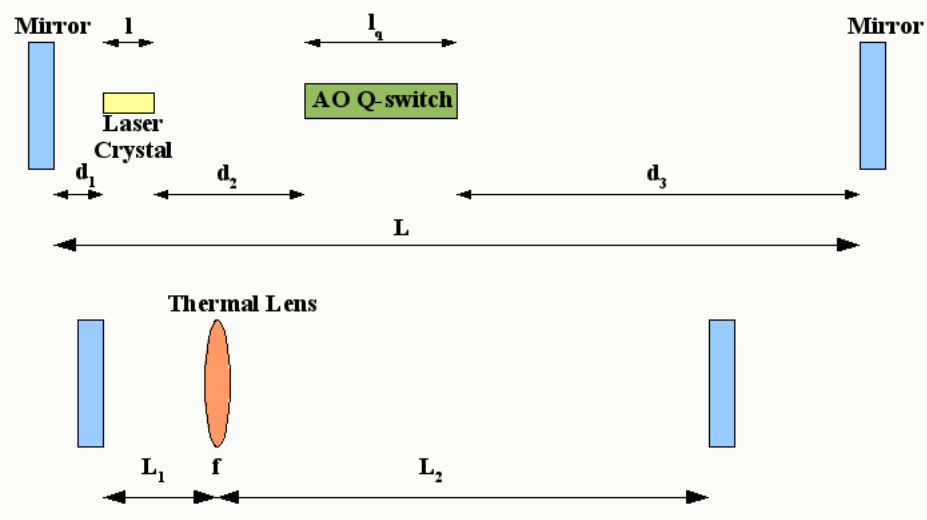

Figure 5.4: (a) Scheme of the laser cavity. (b) Scheme of the equivalent laser cavity

fig. 5.4(b), according to Magni [21], as shown in section 4.3. So,

$$L_1 = d_1 + h = d_1 + \frac{l}{2n} \tag{5.5}$$

and

$$L_2 = h + d_2 + \frac{l_\mathrm{q}}{n_\mathrm{q}} + d_3 = \frac{l}{2n} + d_2 + \frac{l_\mathrm{q}}{n_\mathrm{q}} + d_3 \tag{5.6}$$

where lengths d_1, d_2, L_1 and L_2 are defined according to fig. 5.4, l is the crystal length with refractive index n at the lasing wavelength of 1064 nm, l_q is the length of the acustooptic crystal with refractive index n_q. Being $L_2 > L_1$ and given mirrors curvatures R_1 and $R_2 = \infty$, the stability edges defined in eq. (4.38) become:

$$\frac{1}{f} = \begin{cases} \frac{1}{L_2} \\ \frac{1}{L_1} \\ \frac{1}{L_1} + \frac{1}{L_2} \\ 0 \end{cases} \qquad \Rightarrow \qquad f = \begin{cases} L_2 \\ L_1 \\ \frac{L_1 L_2}{L_1 + L_2} \\ \infty \end{cases} \tag{5.7}$$

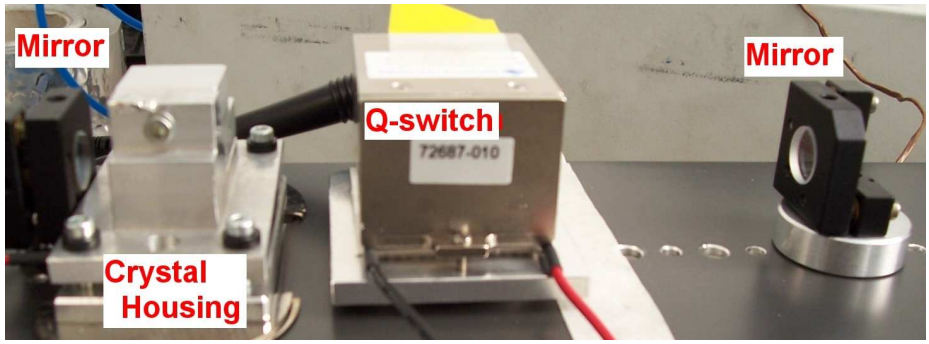

Figure 5.5: Photo of the laser cavity

with stability zone I and stability zone II respectively

$$L_2 < f < \infty \quad ; \quad \frac{L_1 L_2}{L_1 + L_2} < f < L_1 \tag{5.8}$$

with zone II not interesting from a practical point of view. This result gives two indications: (1) the resonator is stable only if the thermal lens is longer than the second branch of the laser cavity, (2) a very simple method to estimate experimentally the thermal lens is by increasing the pump power monitoring when the laser output starts to decrease, there the edge of the stability region is reached and crossed.

An analysis of the cavity misalignment stability can be quickly performed. Given mirrors curvatures R_1 and $R_2 = \infty$, according to the theory shown in section 4.3.3, it is easy to show that

$$S_1 = S_2 = \frac{f}{w_{\text{co}}} = f \left(\frac{\pi}{2\lambda L_2} \right)^{\frac{1}{2}} \tag{5.9}$$

and therefore the overall misalignment sensitivity results

$$S = \left(S_1^2 + S_2^2 \right)^{\frac{1}{2}} = f \left(\frac{\pi}{\lambda L_2} \right)^{\frac{1}{2}} \tag{5.10}$$

Since a plane-parallel resonator gets its mechanical stability thanks to the thermal lensing, it is not surprising that the sensitivity increases as the dioptric power decreases. The previous equation also shows that by fixing

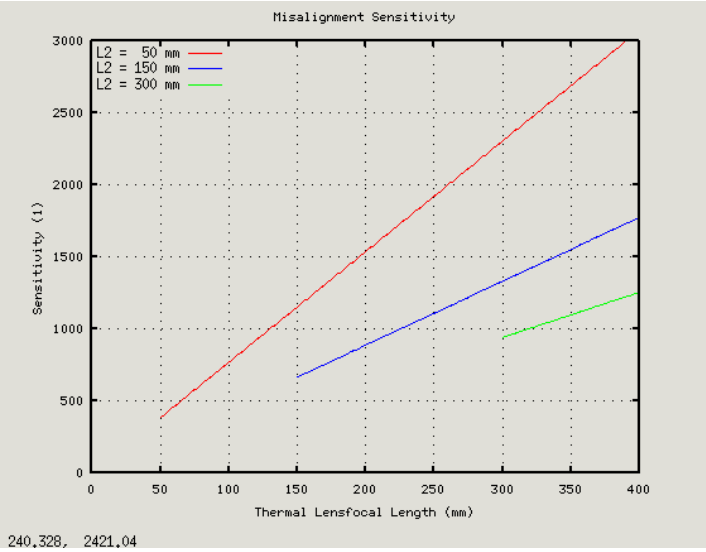

Figure 5.6: Sensitivity dependence on the thermal lensing at various resonator dimensions: L2 is the resonator second branch length. The resonator is stable only if $L_2 < f$.

the resonator second branch length, the sensitivity minimum value is fixed together with its growth rate, see, e.g., graph 5.6.

5.4 Active Medium

A 4x4x10 mm^3 Nd:YVO_4 crystal was chosen and used as active medium, as it was expected to have suitable properties for operation at high frequency ($>$ 50 kHz) and high efficiency. The crystal is a-cut with 0.2 at. % dopant concentration. Vanadate crystals are positive uniaxial, and can therefore be cut along two different directions with the a-cut preferred over the c-cut due to the three times higher absorption; the laser beam will therefore be linearly polarized. The first face of the crystal is AR coated at 1064 nm and 808 nm, the second face is AR coated at 1064 and HR at 808 nm. It is hard to find in literature a crystal with physical parameters similar to those used in this work. In general, shorter crystals (around 4 mm in length) with higher dopant concentration (up to 3 at. %) are used. The present choice tries to find a solution to the problems that always arise in these lasers when scaled to high powers, i.e. the output is limited by undesired thermal

effects and, eventually, crystal fracture. Therefore, the idea is that a longer crystal with lower dopant concentration will have less severe thermal effects, hopefully still showing a high slope efficiency. In particular, a longer crystal has a wider surface and therefore heat removal from the the crystal is faster. A lower dopant concentration guarantees that pump light is absorbed more homogeneously along the gain medium. The crystal absorption coefficient is estimated by an empiric law, found by Peng et al. [24]:

$$\alpha = 2.2\,\rho^{1.4} = 2.2 \cdot 0.2^{1.4} = 0.23\,(\mathrm{mm}^{-1}) \tag{5.11}$$

where ρ is the Nd^{3+} dopant concentration in units of atomic percentage.

5.5 Conclusions

A single-emitters fiber-coupled diode was chosen as the most suitable device for our purpose. It is particularly suitable for the system industrialization, lifetime and power consumption. Test on different coupling configurations showed how equations (4.21) and (4.23) really provide the lowest lasing threshold and the best beam quality. However, at high pump powers, when thermal effects become relevant, a different set-up with bigger pump waist has to be preferred, in order to reach higher output powers. By designing the laser cavity, a simple method to estimate experimentally the thermal lens-focal length was found, and also the misalignment sensitivity was established. A low doped (0.2 at. %) and long (10 mm) crystal was used, in order to verify the theoretical considerations in section 4.1. It must be noted that the pump beam quality was not excellent due to the fiber used for beam delivery. In fact, a "ring" light distribution was observed instead of an expected "top-hat" distribution. This certainly affected the overall laser beam quality, and had to be taken into account.

Chapter 6

Experimental Results

In this chapter several measurements suited to assess the laser source are presented and discussed. In section 6.1 a Nd:YVO_4 crystal (4x4x10 mm^3, 0.2 at. % dopant concentration) is used as active media in different configurations. In section 6.2 a Nd:YVO_4 crystal (3x3x15 mm^3, 0.2 at. % dopant concentration) is used in a set-up with cavity length $L = 150$ mm and thermoelectric cooling. In section 6.3 a Nd:$GdVO_4$ crystal (3x3x15 mm^3, 0.2 at. % dopant concentration) is used in place of the vanadate crystal of section 6.2. In section 6.4 the performance of the developed source are evaluated and compared with other technologies.

6.1 Nd:YVO_4 4x4x10 mm^3

At first, a traditional water-cooled set-up was built and investigated. If promising results were to be obtained, then an effort would be done in order to get the same results with an air-cooled set-up.
So, in the first experiment, the gain medium was hosted in a water-cooled aluminum housing, where water temperature was maintained at 16 ℃. Later, the water-cooling system was replaced with a thermoelectric cooler device. The TEC transferred heat from the crystal housing to a fan cooled heat sink.

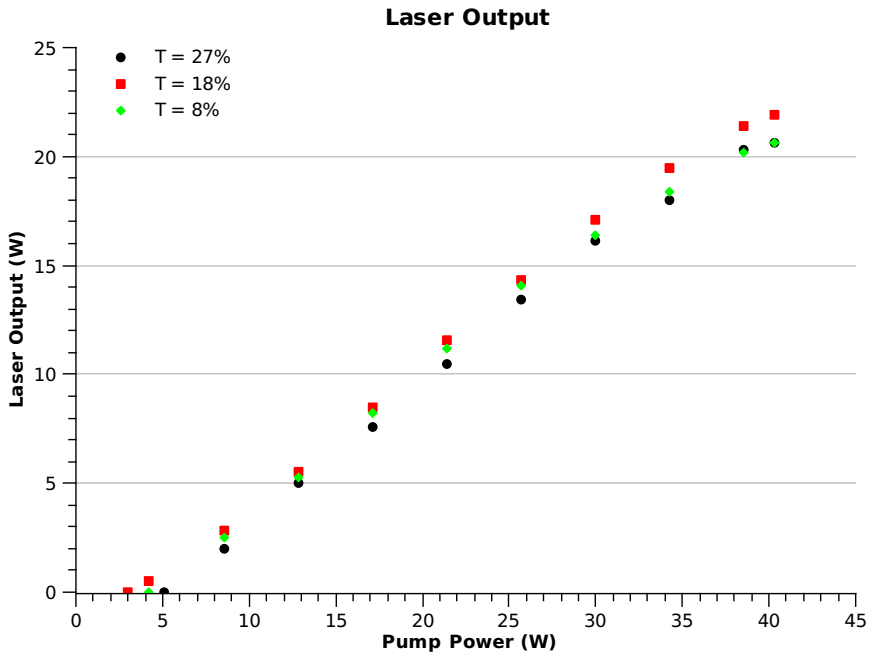

Figure 6.1: Laser output at different output mirrors transmissivity. Cavity length is $L = 103$ mm

6.1.1 Cw Behavior and Thermal Lensing

Firstly, a suitable value for the output mirror transmissivity needed to be estimated. Three mirrors with transmissivity T_1= 27%, T_2= 18% and T_3= 8% were available to test. The laser output at the three different arrangements is plotted in fig. 6.1. The mirror with transmissivity T=18% showed highest slope efficiency and lowest threshold and was therefore found to be the most suited.

Measurement were carried out to verify equation (4.27) and to define the value of the correction factor r_f. The method to determine the thermal lens was found in section 5.3: the thermal lens corresponds to the length of the laser cavity second branch at the pump power where the maximum output power is reached. Therefore, the input/output relation at several cavity length was measured. The results are plotted in fig. 6.2. The measurement was repeated when water-cooling was replaced with the TEC system, and the result is plotted in fig. 6.3. Relevant data extrapolated from the plots are

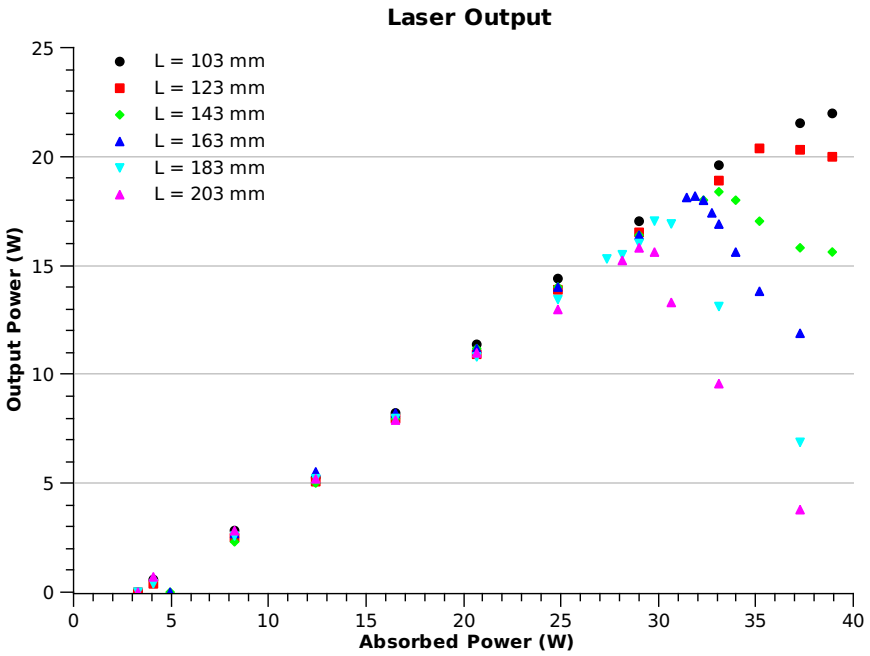

Figure 6.2: Laser output at different cavity lengths. (Water-cooling)

summarized in table 6.1. It must be noted that the pump power absorbed by the gain medium coincides with the input power, thanks to the high-reflectivity coating at 808 nm on crystal second face. In turn, the input power $P_{\mathrm{in}} = P_{\mathrm{p}} * (1 - c_{\mathrm{l}}) = P_{\mathrm{abs}}$ where P_{p} is the diodes pump power and $c_{\mathrm{l}} = 3.3\%$ are the coupling losses.

Lower output powers measured in the air-cooled set-up are likely to be addressed to less efficient heat removal. Anyway, slope efficiency is very close in both set-ups, reaching 64%. Therefore it is clear how tit is possible to build an efficient, compact, air-cooled system.
The value of the dioptric power $1/f$ is very useful to verify the linearity of eq. (4.27), which can be written as follows:

$$\frac{1}{f} = \frac{A_0}{2\pi K_{\mathrm{c}}} \frac{\xi}{\bar{w}_{\mathrm{p}}^2} \frac{1}{r_f} P_{abs} = \frac{\kappa}{r_f} P_{abs} \tag{6.1}$$

where $\kappa = \frac{A_0}{2\pi K_{\mathrm{c}}} \frac{\xi}{\bar{w}_{\mathrm{p}}^2}$ includes all physical constants. See data plotted in fig.

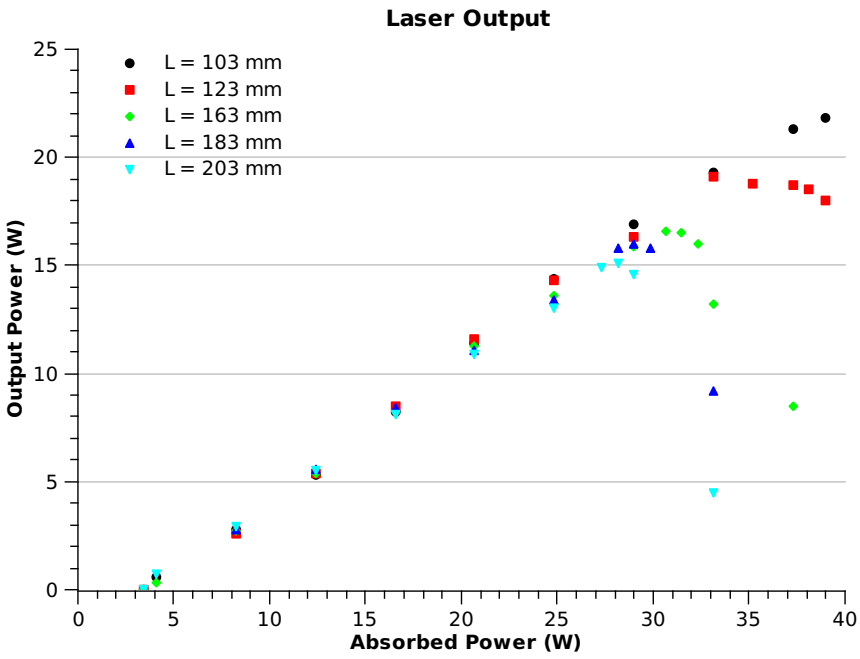

Figure 6.3: Laser output at different cavity lengths. (Thermoelectric cooling)

	L (mm)	max(P_{out}) (W)	P_{abs} (W)	$L_2 = f$ (mm)	$1/f$ (mm^{-1})
Water - cooling	103	not reached			
	123	20.4	35.21	103.7	0.00964
	143	18.3	33.14	123.7	0.00808
	163	18.2	31.48	143.7	0.00696
	183	17	29.82	163.7	0.00611
	203	15.8	28.99	183.7	0.00544
Thermoelectric cooling	103	not reached			
	123	19.1	33.14	97.7	0.01024
	163	16.6	30.65	137.7	0.00726
	183	16	28.99	157.7	0.00634
	203	15.1	28.16	177.7	0.00563

Table 6.1: Thermal lens values at different pump powers. Differences in the values of L_2 are due to the slightly different distance d_1 in the two set-ups.

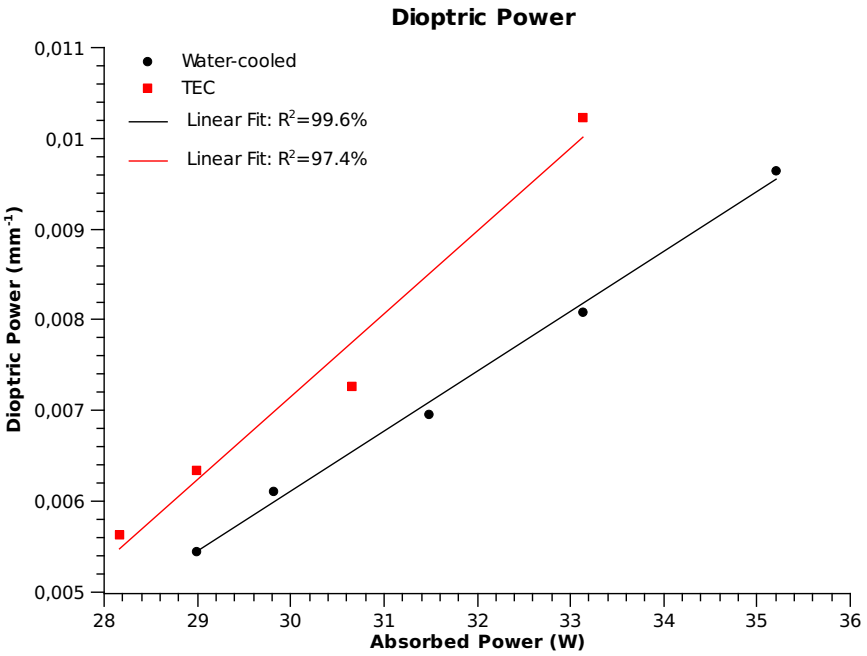

Figure 6.4: Dioptric power at different pump powers in the two set-ups.

6.4.

It is interesting to verify if the theoretical prediction is close to the measured values. Physical constants for Nd:YVO_4 are: $K_c = 0.00523$ W/(mm K), $\delta n/\delta T = 2.9 \cdot 10^{-6}$ K^{-1}, $n_e = 2.1652$, $\nu = 0.33$ [25], $\alpha_T = 4.43 \cdot 10^{-6}$ K^{-1}. $C_r = 0$ because of the crystal natural birefringence. So, according to eq. (4.26), $A_0 = 9.765 \cdot 10^{-6}$ K^{-1}. The fractional thermal loading ξ depends on dopant concentration. Its value was estimated from measurements by Peng et al. [24], and was found to be $\xi = 0.222$ at continuous wave operation. The average pump beam radius can be found with equation (4.18) and results $\bar{w}_p = 0.481$ mm. Finally, the theoretical value for κ results $\kappa = 284 \cdot 10^{-6}$ (mm W)$^{-1}$. Experimental and theoretical values are shown in table 6.2 for quick comparison. The theoretical value is found to be close to the measured values. But, as it is evident from the chart, the measured values have a linear dependence on the cavity length or, more exactly, on the ratio between the laser beam dimension in the crystal and the average pump beam radius, as proved by Fan et al. [23]. In the present set-up, eq.

$\kappa = 284 \cdot 10^{-6}$	L (mm)	$\frac{1}{f}$ (mm^{-1})	κ_m (mm W)$^{-1}$	$w_\mathrm{c}/\bar{w}_\mathrm{p}$	$r_\mathrm{f} = \kappa/\kappa_\mathrm{m}$
Water - cooling	123	0.00964	$274{\cdot}10^{-6}$	0.551	1.04
	143	0.00808	$244{\cdot}10^{-6}$	0.602	1.16
	163	0.00696	$218{\cdot}10^{-6}$	0.649	1.30
	183	0.00611	$205{\cdot}10^{-6}$	0.692	1.39
	203	0.00544	$188{\cdot}10^{-6}$	0.733	1.51
Thermoelectric cooling	123	0.01024	$309{\cdot}10^{-6}$	0.535	0.92
	163	0.00726	$237{\cdot}10^{-6}$	0.635	1.20
	183	0.00634	$219{\cdot}10^{-6}$	0.680	1.30
	203	0.00563	$200{\cdot}10^{-6}$	0.721	1.42

Table 6.2: Correction factor r_f for eq. (4.27), in the two different set-ups

(4.43) becomes

$$w_\mathrm{c} = \left\{ \frac{2\lambda}{\pi} \left[\min \left(\left| \frac{1}{u_1} \right|, \left| \frac{1}{u_2} \right| \right) \right]^{-1} \right\}^{\frac{1}{2}} = \left(\frac{2\lambda L_2}{\pi} \right)^{\frac{1}{2}} \tag{6.2}$$

The ratio $w_\mathrm{c}/\bar{w}_\mathrm{p}$ is reported in table 6.2 and the linear correlation with r_f is shown in fig. 6.5. The linear fit of the data gives the relations:

$$r_\mathrm{f} = 2.57 \cdot \frac{w_\mathrm{c}}{\bar{w}_\mathrm{p}} - 0.38 \tag{6.3}$$

and

$$r_\mathrm{f} = 2.62 \cdot \frac{w_\mathrm{c}}{\bar{w}_\mathrm{p}} - 0.48 \tag{6.4}$$

for the water-cooled set-up and the thermoelectric cooled set-up respectively.

6.1.2 Beam Quality

Laser beam quality was evaluated both qualitatively, by observing the laser spot with a camera, and quantitatively by measuring the M^2 parameter. Images of the laser beam were taken by means of a CCD camera (FX 50, Ophir-Spiricon Inc.) at different powers for several cavity lengths (water-cooled set-up). A few examples are shown in figures 6.6 up to figures

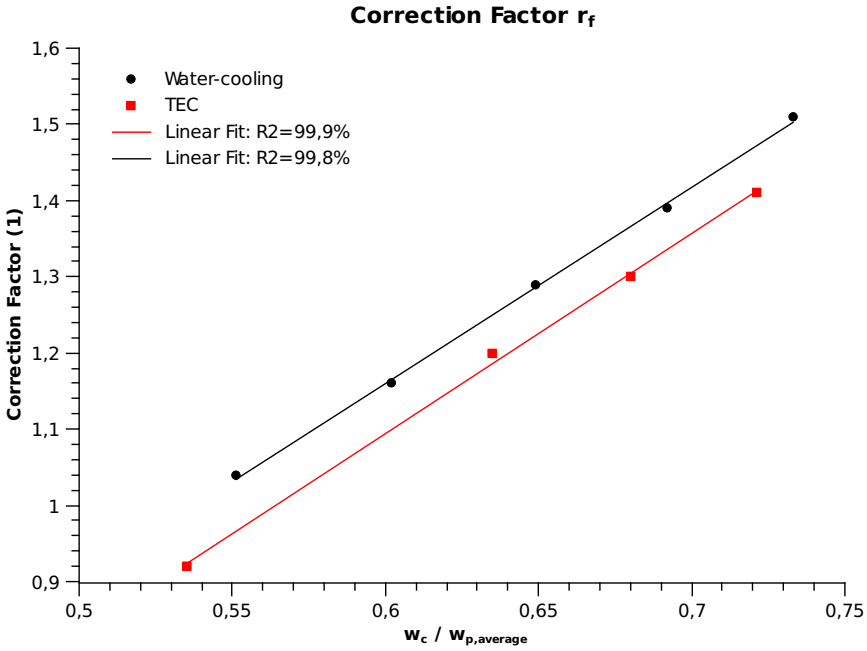

Figure 6.5: Correction factor as function of laser mode/pump mode ratio in the two set-ups.

6.13. The camera software automatically recognizes the beam and shows the center of the centroid, the peak position, a 3D reconstruction and the beam profile on horizontal and vertical directions.

Measurements to estimate the value of the M-square parameter were performed. Knife-edge technique was used to evaluate the beam radius at different positions and from this values the Gaussian beam propagation law was interpolated to estimate laser beam waist and M^2 value. Knife-edge technique is a beam profiling method that allows for quick and accurate determination of the cross-sectional laser beam parameters. A sharp edge (e.g. a razor blade) was translated perpendicular to the direction of propagation

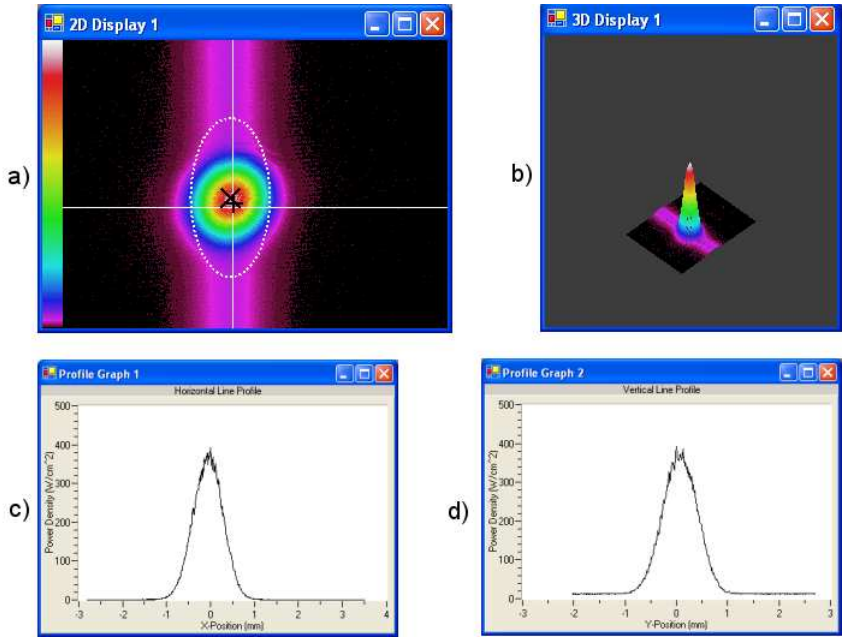

Figure 6.6: Laser spot: a) 2D image b) 3D reconstruction c) horizontal and d) vertical profile graph. Cavity length $L = 143$ mm, output power $P_{\text{out}} = 2.3$ W.

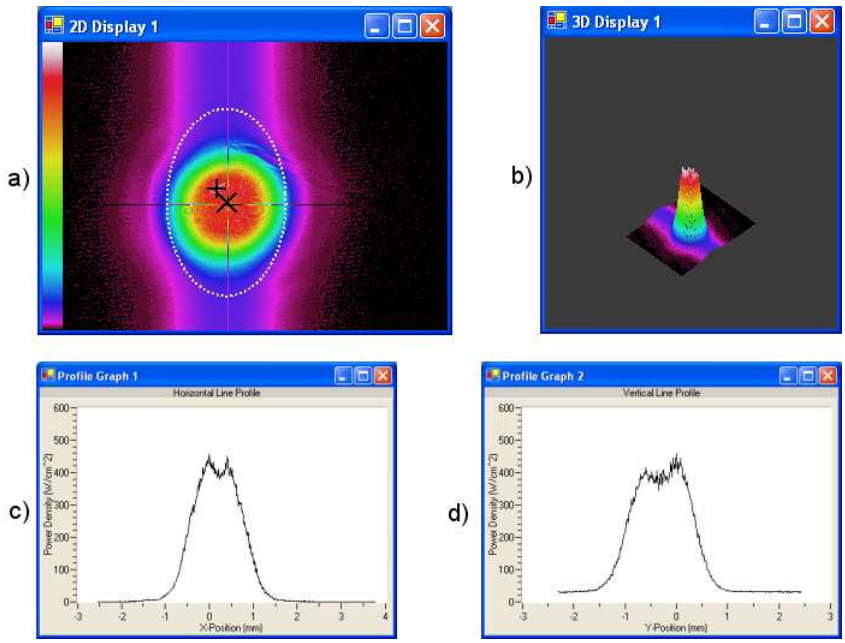

Figure 6.7: Laser spot: a) 2D image b) 3D reconstruction c) horizontal and d) vertical profile graph. Cavity length $L = 143$ mm, output power $P_{\text{out}} = 8.0$ W.

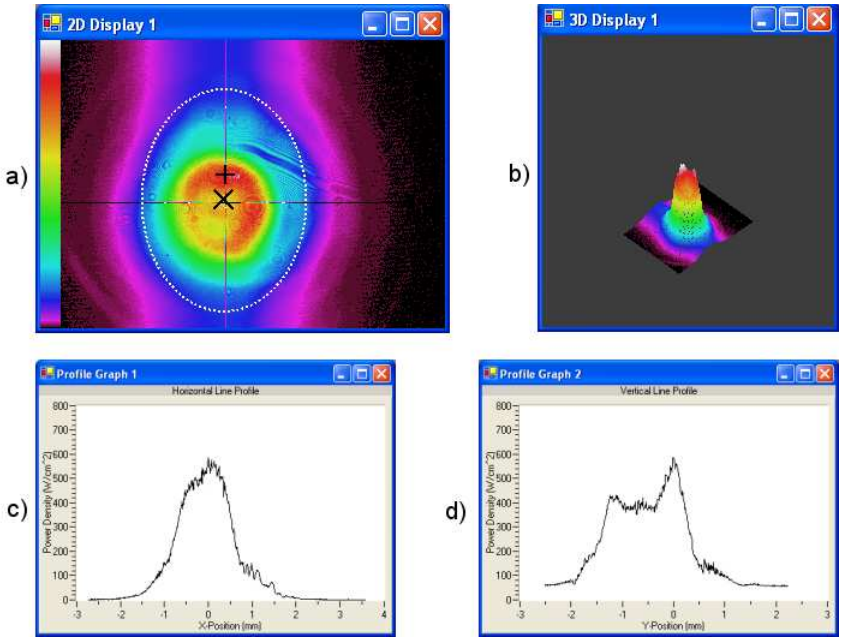

Figure 6.8: Laser spot: a) 2D image b) 3D reconstruction c) horizontal and d) vertical profile graph. Cavity length $L = 143$ mm, output power $P_{\text{out}} = 14.0$ W.

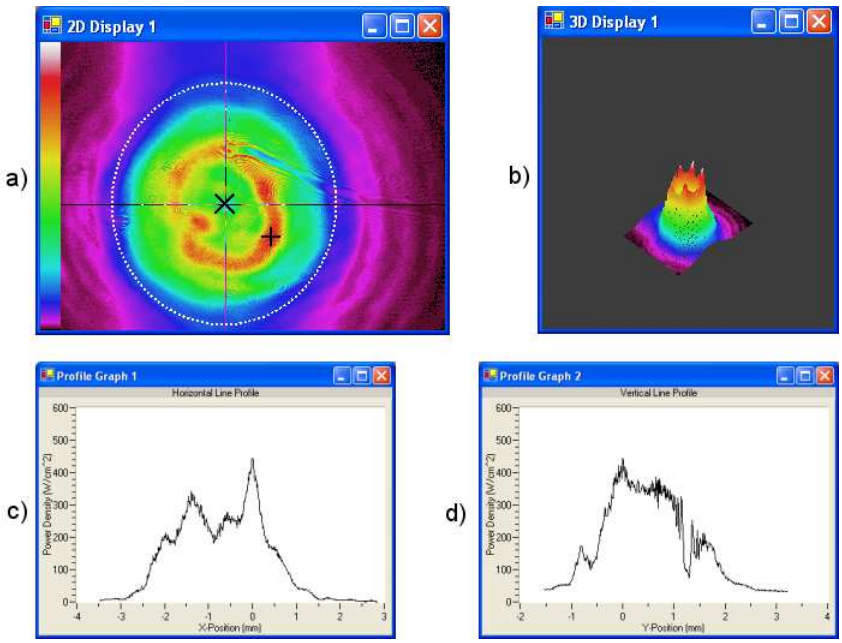

Figure 6.9: Laser spot: a) 2D image b) 3D reconstruction c) horizontal and d) vertical profile graph. Cavity length $L = 143$ mm, output power $P_{\text{out}} = 17.9$ W. Stability margin.

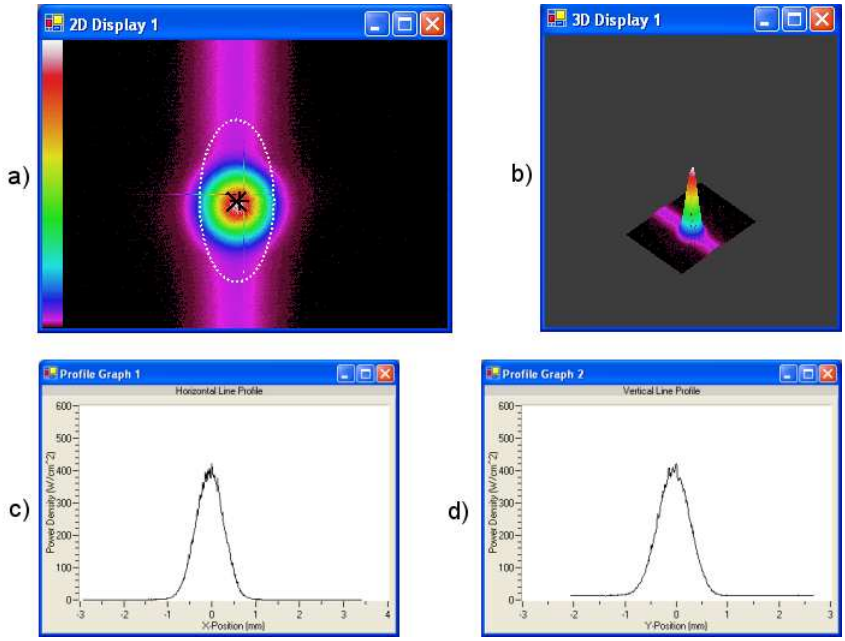

Figure 6.10: Laser spot: a) 2D image b) 3D reconstruction c) horizontal and d) vertical profile graph. Cavity length $L = 183$ mm, output power $P_{\text{out}} = 2.9$ W.

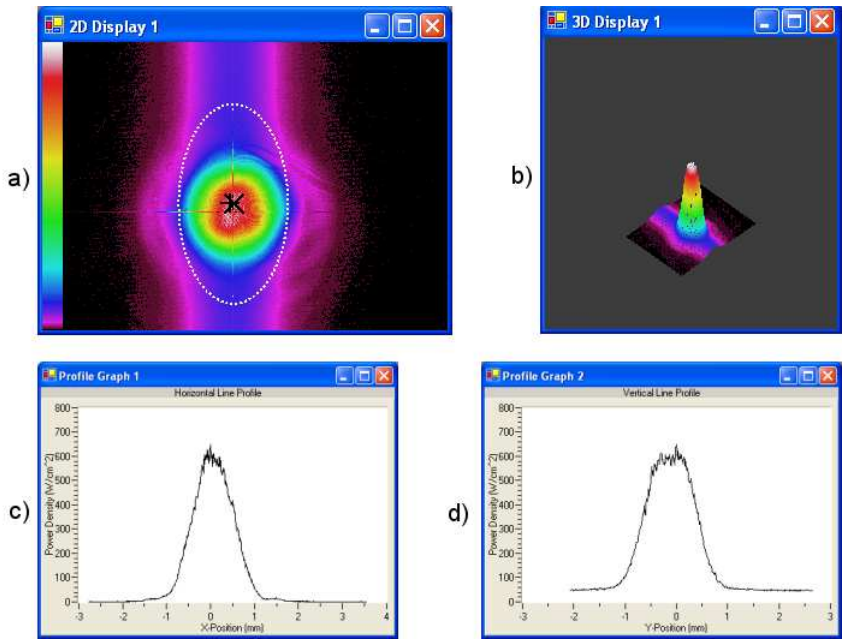

Figure 6.11: Laser spot: a) 2D image b) 3D reconstruction c) horizontal and d) vertical profile graph. Cavity length $L = 183$ mm, output power $P_{\text{out}} = 7.9$ W.

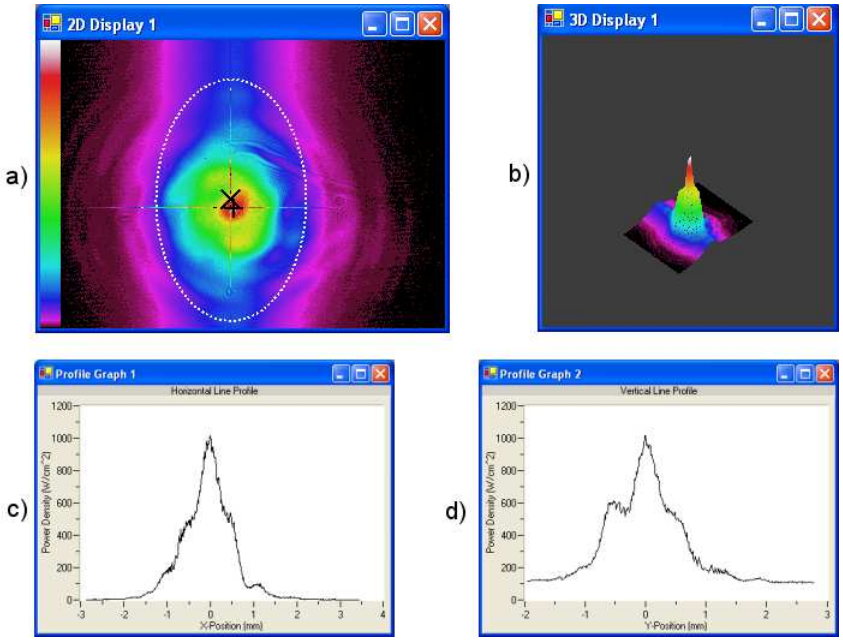

Figure 6.12: Laser spot: a) 2D image b) 3D reconstruction c) horizontal and d) vertical profile graph. Cavity length $L = 183$ mm, output power $P_{\text{out}} = 13.2$ W.

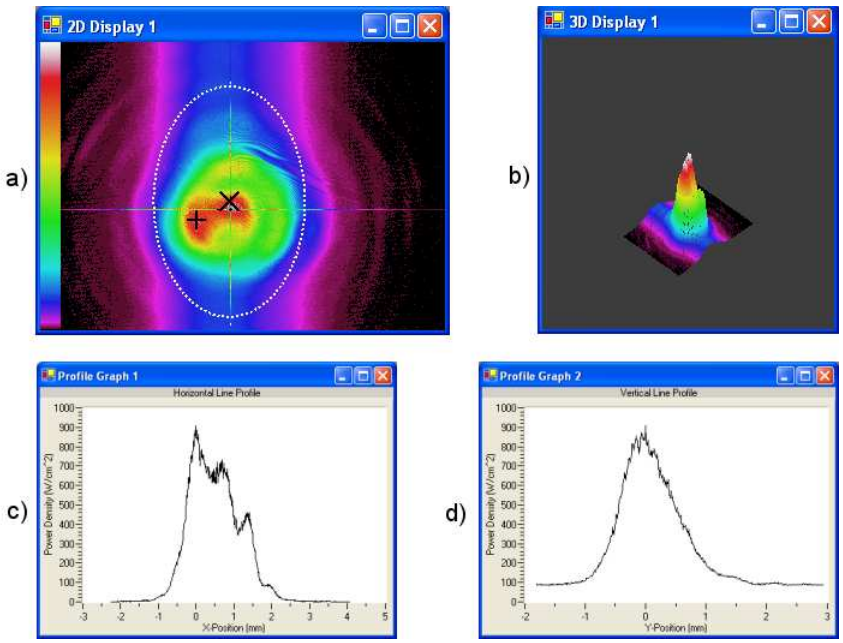

Figure 6.13: Laser spot: a) 2D image b) 3D reconstruction c) horizontal and d) vertical profile graph. Cavity length $L = 183$ mm, output power $P_{\text{out}} = 16.4$ W. Stability margin.

of the laser beam at micrometric steps. The blade is initially covering the laser beam, and at each step, the power meter shows an increase in total power until the entire beam is detected. The collected data represents the Gaussian profile integrated over the displacement of the razor blade (see fig. 6.14[a]) Therefore, the derivative at each point was taken by averaging the derivative of two adjacent data points:

$$\frac{dP}{dx} = \frac{1}{2}\left(\frac{y_{i+1} - y_i}{x_{i+1} - x_i} + \frac{y_i - y_{i-1}}{x_i - x_{i-1}}\right) \tag{6.5}$$

so that the beam Gaussian profile is reconstructed (see fig. 6.14[b]). Then, a Gaussian of the kind

$$I(x) = A\exp\left[-\frac{2(x - x_0)^2}{r^2}\right] \tag{6.6}$$

where r is the beam radius at $1/e^2$, was fit to the data. Each step of the micrometric screw was 100 μm. The derivative was easily calculated by using a spreadsheet, while the Gaussian fit was evaluated with the open source analysis program QtiPlot. It must be noted that the r^2 parameter for each fit was very high, always over 94%.

The knife-edge technique was applied on the laser cavity of length $L =$ 153 mm (TEC set-up). Four different beam profiles at different distances from the output mirror were collected, for several output powers. The data were then fit with the propagation law of Gaussian beams,

$$w = \left[w_0^2 + \left(M^2\frac{\lambda(z - z_0)}{\pi w_0}\right)^2\right]^{\frac{1}{2}} \tag{6.7}$$

where $z_0 = 0$ coincides with the output mirror, in order to evaluate the M^2 parameter and the beam waist w_0. Results are summarized in table 6.3.

6.1.3 Pulsed Behavior

It is important to verify the laser behavior in pulsed regime. Especially, it must be verified to have short and uniform laser pulses with adequate

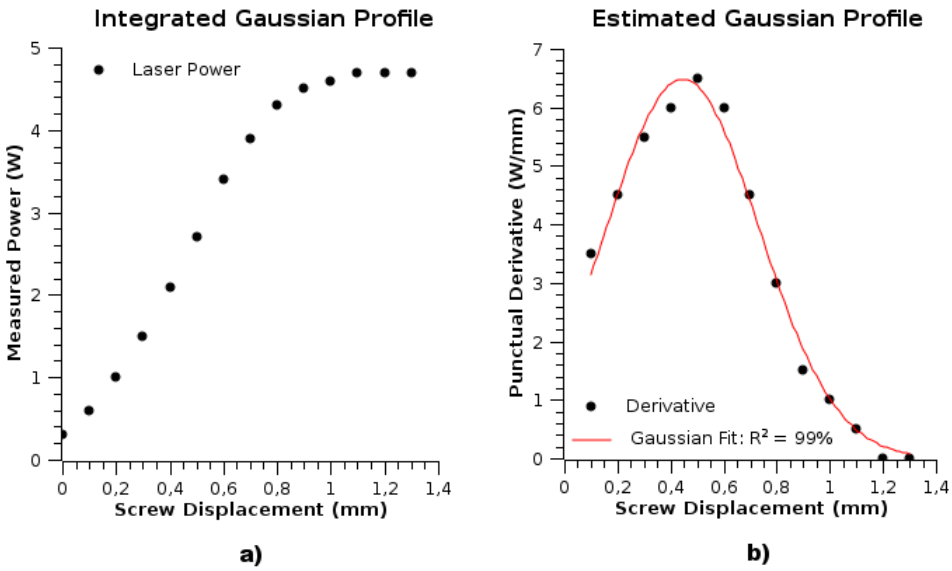

Figure 6.14: Knife-edge technique. a) Measured power draws the integral of a Gaussian b) the Gaussian profile is reconstructed by taking the derivative at each point

P_{in}	P_{out}	$w(z=330)$	$w(z=430)$	$w(z=530)$	$w(z=630)$	w_0	M^2
12.4	4.7	0.575	0.648	0.727	0.860	0.415	1.4
16.6	7.5	0.718	0.856	1.014	1.168	0.438	2.2
20.7	10.0	0.811	1.005	1,187	1.353	0.474	2.8
24.8	12.3	0.972	1.187	1.393	1.598	0.590	3.2
26.9	13.0	0.724	0.903	1.124	1.334	0.195	1.2
29.0	14.6	0.838	1.114	1.361	1.638	0.133	1.1

Table 6.3: Estimate of laser waists at different powers and positions, with estimate of beam waist w_0 and M^2 parameter. Laser powers are expressed in watts, waist dimensions and distances z in millimeters. Cavity length was 153 mm, TEC set-up.

f (kHz)	1	5	10	15	20	30	40	50	60
P_{av} (W)	0.8	3.3	5.6	6.9	8.0	9.3	10.1	10.4	10.8
τ (ns)	13.5	14.5	15.5	20.0	24.0	31.5	38.0	40.0	43.0
E_{i} (mJ)	0.80	0.67	0.56	0.46	0.40	0.31	0.25	0.21	0.18
P_{peak} (kW)	59.3	45.5	36.1	23.0	16.7	9.8	6.6	5.2	4.2
σ (%)	< 5	< 5	< 5	< 5	< 5	< 5	< 5	< 5	< 10

Table 6.4: Nd:YVO_4 4x4x10 mm^3: pulses properties at different working frequencies f. P_{av} is the average power, τ is the pulse FWHM, $E_{\mathrm{i}} = P_{\mathrm{av}}/f$ is the energy per pulse, $P_{\mathrm{peak}} = E_{\mathrm{i}}/\tau$ is a rough estimate of pulse peak power and σ is pulse FWHM standard deviation. Cavity length is 163 mm

energy and peak power. The laser cavity is equipped with an acustooptical Q-switch, producing pulses up to 100 kHz in frequency. A logic signal controls the commutation of a radiofrequency generator (RF) from a high level (on) to a low level (off): when the signal is high, a 41 MHz radiofrequency is applied to a piezoelectric transducer generating a compressional wave in a crystal quartz. The strain induced by the ultrasonic wave results in local changes in the material refractive index due to photoelastic effect. This periodic change acts as a phase grating diffracting a fraction of the laser beam from the incident beam direction. The increase in cavity losses prevents lasing action, while population inversion increase up to saturation due to pump light. When the logic signal is lowered, the radiofrequency turns off giving rise to a short (nanoseconds range) and high-power (kilowatts range) laser pulse. A simple set-up to measure pulses dimensions was arranged: the laser pulses were directed toward a metallic surface. By means of a fast photodiode (Alphalas, sensitivity range 320-1100 nm, rise time < 1 ns) the light backscattered from the metallic target is acquired and the pulses temporal profile is reconstructed. The signal from the photodiode was analyzed with an oscilloscope (Tektronix TDS3054B). Several measurements on the two set-ups (water-cooled and thermoelectric cooled), were performed. The results were very similar and could be therefore averaged without loss of information (see table 6.4).

6.1.4 Results Analysis

In continuous wave operation, the laser shows a very high efficiency in both the set-ups, with slope efficiency reaching 64% and optical-to-optical efficiency reaching 54%. It must be noted that this excellent result is obtained despite the low dopant percentage in the crystal. This gives a first validation of our early intuition, i.e., high dopant concentration is not necessary to reach high efficiencies.

Thermal lens measurements are in good agreement with Innocenzi's formula, and they also support Fan's results. In fact, a correction in Innocenzi's formula is needed to properly evaluate the thermal lens-focal length. The correction here found, see eq. (6.3) and (6.4), is close to the correction proposed by Fan, but it is not directly comparable. In fact, Fan's work was verified in a short range at low input powers (1 W $< P_{\text{in}} <$ 3 W), and relies on the hypothesis:

$$\frac{\xi A_0}{4\pi K_c} P_{abs} << 10^{-4}$$

which is not satisfied in this work, where, on the contrary,

$$\frac{\xi A_0}{4\pi K_c} P_{abs} > 10^{-4}$$

In figure 6.15 it is shown the thermal lens-focal length, for a 150 mm cavity length, evaluated according to Innocenzi's formula (4.25) and according to our corrections (equations (4.27) and (6.3) for the water cooled set-up). The corrected focal length is 20% longer than the prediction by Innocenzi. So, our result integrates and strengthen Fan's work and further demonstrates the need of a correction for Innocenzi's formula, wishing for a more general and analytical solution to the problem. The different correction factors found between the two set-ups indicate a difference in heat removal efficiency, with TEC set-up giving a lower performance.

Both the measurements on beam quality, i.e., the measure of the M^2 via the knife-edge technique and the beam profile reconstruction with the CCD camera software, show that the beam is close to a TEM_{00} mode only

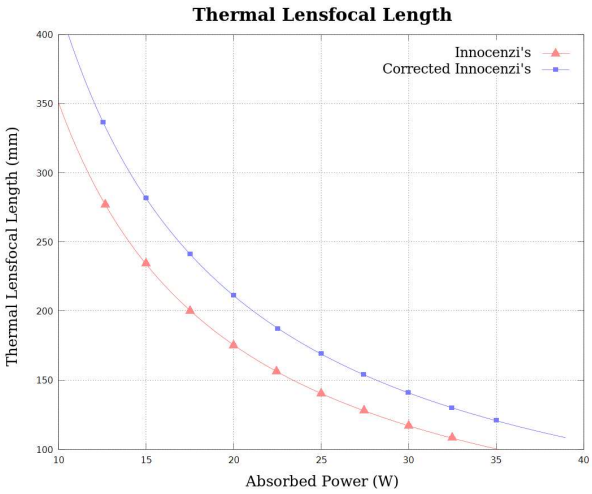

Figure 6.15: Comparison among thermal lens-focal length evaluated with Innocenzi's formula and corrected Innocenzi's.

at low powers, and quickly falls into higher modes as input power increases. Such fast degradation was clearly not wanted. The main reasons behind this behavior are probably to be found in a not sufficient heat removal rate and in the poor pump beam quality, as discussed in chapter 5.1.
The data reported in table 6.4 are very satisfying already at this early stage. Pulse length is not longer than 50 ns even at high frequencies, and the pulse repeatability is excellent, being the standard deviation less than 5% over a wide frequency range. The pulses peak powers are high enough to guarantee a good material removal on many different surfaces.

As the results here obtained are promising for a laser source suitable for the desired aims, the efforts will be now directed toward the attainment of a better beam quality and possibly a higher average power. This will be mainly possible by two ways, the use of a different fiber for the coupling of light from the diode to the active medium, and by reducing the thermal effects arising in the laser crystal.

6.1.4.1 Thermal Analysis

Crystal heating is an important contributor in beam quality degradation. It is therefore interesting and useful to build an analytical model suitable

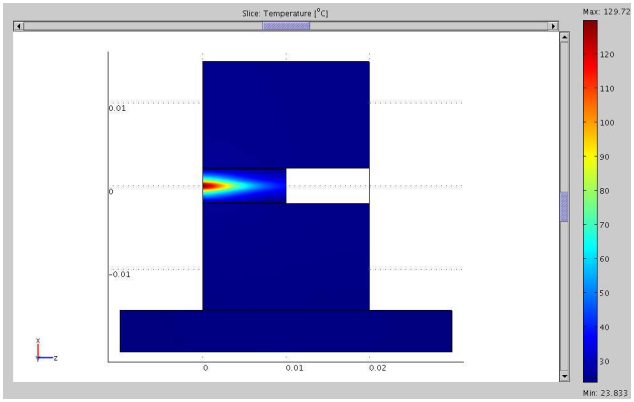

Figure 6.16:]
FEM simulation of temperature profile for the crystal housing.

to evaluate heat distribution inside the crystal. Pump radiation can be considered as a steady heat source with a "top-hat" distribution. This applies heat generation rates to the crystal (heat flow rate per unit volume) as [25]

$$
\begin{aligned}
q(x,y,z) &= \xi P_0\, r_{\mathrm{p}}(x,y,z) \qquad (6.8)\\
r_{\mathrm{p}}(x,y,z) &= \frac{\alpha\, e^{-\alpha z}}{\pi w_{\mathrm{p}}(z)^2}\mathrm{H}(w_{\mathrm{p}}^2(z) - x^2 - y^2)\\
w_{\mathrm{p}}^2(z) &= w_{\mathrm{po}}^2\left\{1 + \left[M^2\frac{\lambda_{\mathrm{p}}(z-z_0)}{\pi n_{\mathrm{p}} w_{\mathrm{po}}^2}\right]^2\right\}
\end{aligned}
$$

where $r_{\mathrm{p}}(x,y,z)$ is the normalized pump radiation distribution and differs from eq. (4.7) because of the HR coating at 808 nm on crystal end face. It is helpful to apply this analytical description into a Finite-Element Model. The accuracy of the FE analysis depends on the numerical solution of the algorithm and the values of the input parameters, such as material thermo-dynamic properties and boundary conditions. In the thermo-electric cooled set-up, the boundary conditions to the crystal housing are set to a heat flux proportional to the heat transfer coefficient of air for all the surfaces except the one in contact with the TEC. Here a constant outward flux is fixed. The proprietary software COMSOL Multyphysics was used for the calculations.

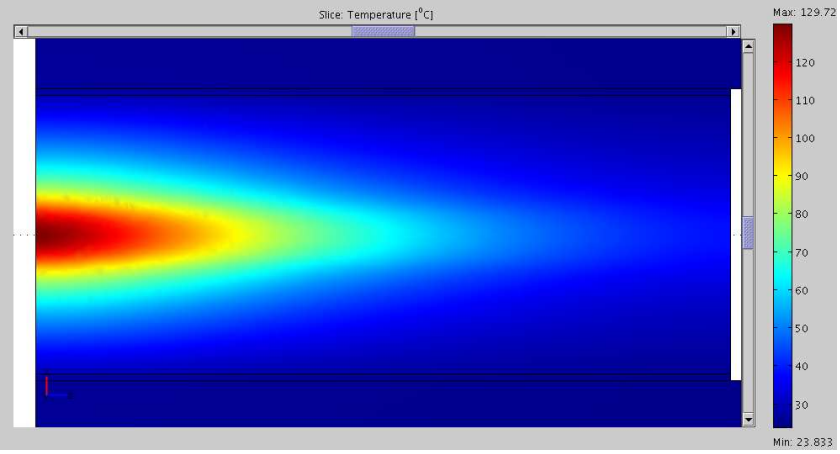

Figure 6.17: FEM simulation of temperature profile: zoom on the 4x4x10 mm^3 crystal

Simulation results are shown in figure 6.16 and figure 6.17. These are in good agreement with the measured values, in fact an almost constant temperature of 25 ℃ was found on the outer Cristal housing faces. The graph shows a temperature peak on crystal entrance face and a quick temperature drop in both axial and radial directions (see also figure 6.18).

A way to reduce the maximum temperature and smoothen its distribution in the crystal is to use an active medium smaller in cross section and longer in length. The reduced cross section will result in a more efficient heat removal from the crystal center, the longer dimension will allow to move the pump focus slightly deeper in the crystal and to have a wider surface for heat removal. Therefore, a simulation on a crystal with dimension 3x3x15 mm^3 was performed, and the results are shown in figures 6.19 and 6.20. As can be seen from the plots, such a crystal should have a 13 ℃ lower maximum temperature. On the other hand it must also be noted that the temperature gradient is slightly higher for the 3 mm wide crystal (30.7 ℃/mm against 26.3 ℃/mm) and the effects must be evaluated experimentally. A further reduction in the crystal cross section is not recommendable, because the wings of the oscillating modes would be cut away, leading to undesired diffraction effects.

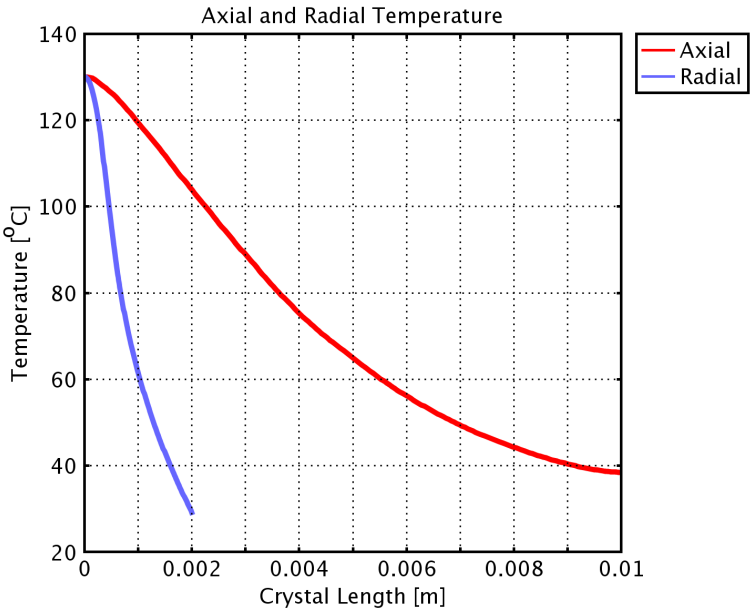

Figure 6.18: Radial and axial crystal temperature profiles in the 4x4x10 mm^3 crystal.

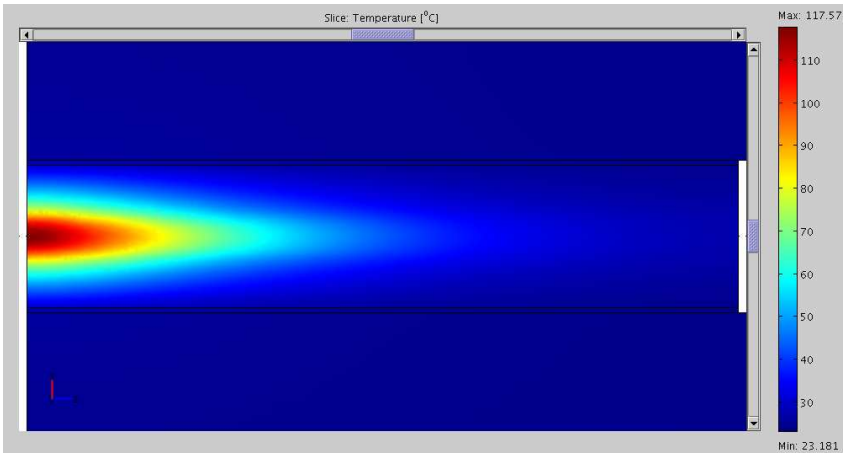

Figure 6.19: FEM simulation of temperature profile in the 3x3x15 mm^3 crystal.

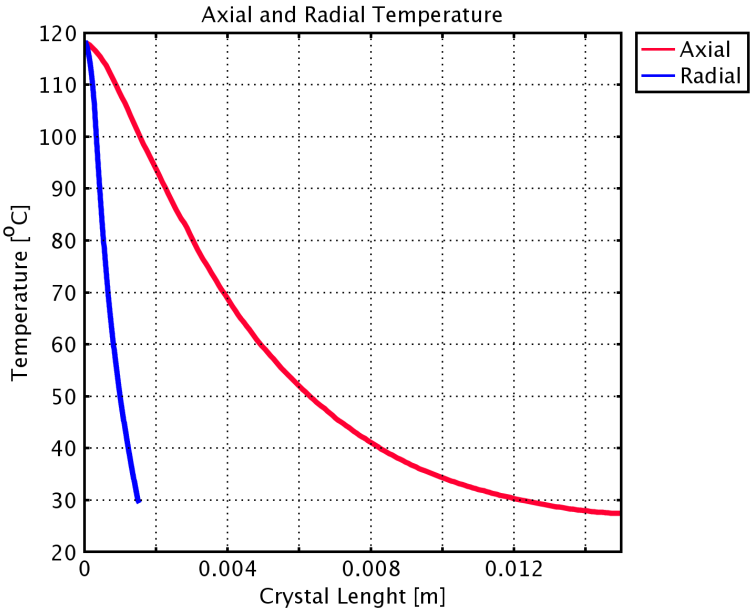

Figure 6.20: Radial and axial crystal temperature profiles in the 3x3x15 mm^3 crystal.

6.2 Nd:YVO_4 3x3x15 mm^3

As a consequence of the previous considerations, a second laser crystal was purchased by the company, and was therefore available for testing. The new crystal is a Nd:YVO_4, 3x3x15 mm^3 with 0.2 at. % dopant concentration. The first face of the crystal is AR coated at 1064 nm and 808 nm, the second face is AR coated at 1064 and HR at 808 nm. Cavity length was fixed to $L = 150$ mm and thermoelectric cooling was implemented. Measurements on laser output, beam quality and dynamic behavior were performed with the same methods discussed in previous section. The results are here presented. See figures 6.21 - 6.25 and tables 6.5, 6.6.

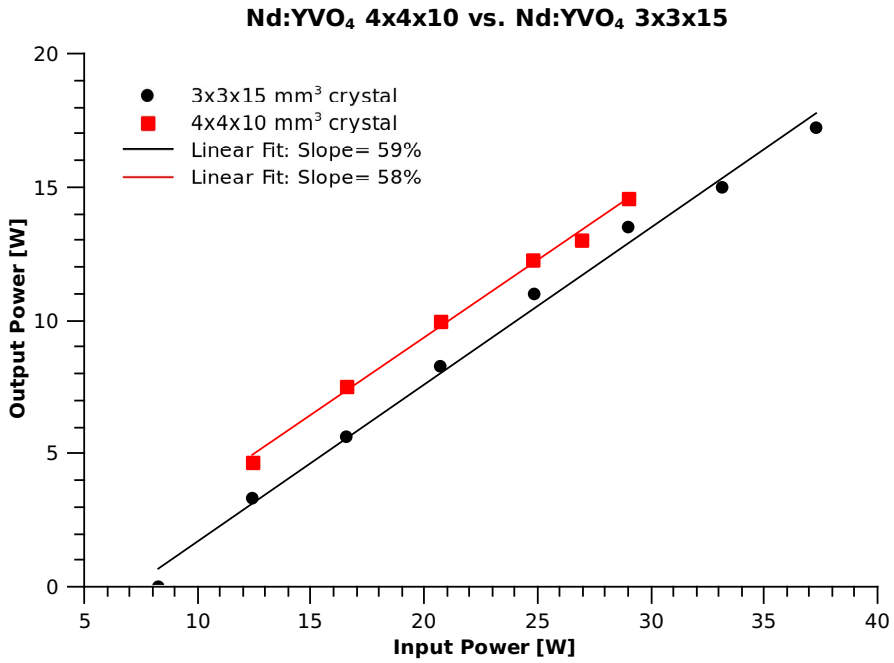

Figure 6.21: Laser input/output relation.

	P_{in}	P_{out}	$w_{z=215}$	$w_{z=365}$	$w_{z=415}$	$w_{z=615}$	w_0	M^2
cw	22.4	10.1	0.641	0.858	0.944	1.287	0.488	2.8
Pulsed	22.4	9.3	0.508	0.728	0.821	1.118	0.354	1.8

Table 6.5: Estimation of laser waists at different powers and positions, with estimate of beam waist w_0 and M^2 parameter. Laser powers are expressed in watts, waist dimensions and distances z in millimeters. The working frequency in pulsed regime is $f = 50$ kHz.

f (kHz)	1	5	10	15	20	30	40	50	70
P_{av} (W)	0.5	2.1	3.9	5.7	7.1	8.2	8.7	8.9	9.6
τ (ns)	8.2	7.7	9.6	12.0	14.0	17.0	19.0	20.0	32.0
E_{i} (mJ)	0.50	0.42	0.39	0.38	0.36	0.27	0.22	0.18	0.14
P_{peak} (kW)	61.0	54.5	40.6	31.7	25.4	16.1	11.4	8.9	4.3
σ (%)	< 5	< 5	< 5	< 5	< 5	< 5	< 5	< 5	< 10

Table 6.6: Nd:YVO$_4$ 3x3x15 mm^3: pulses properties at different working frequencies f. P_{av} is the average power, τ is the pulse FWHM, $E_{\text{i}} = P_{\text{av}}/f$ is the energy per pulse, $P_{\text{peak}} = E_{\text{i}}/\tau$ is a rough estimate of the pulse peak power and σ is pulse FWHM standard deviation.

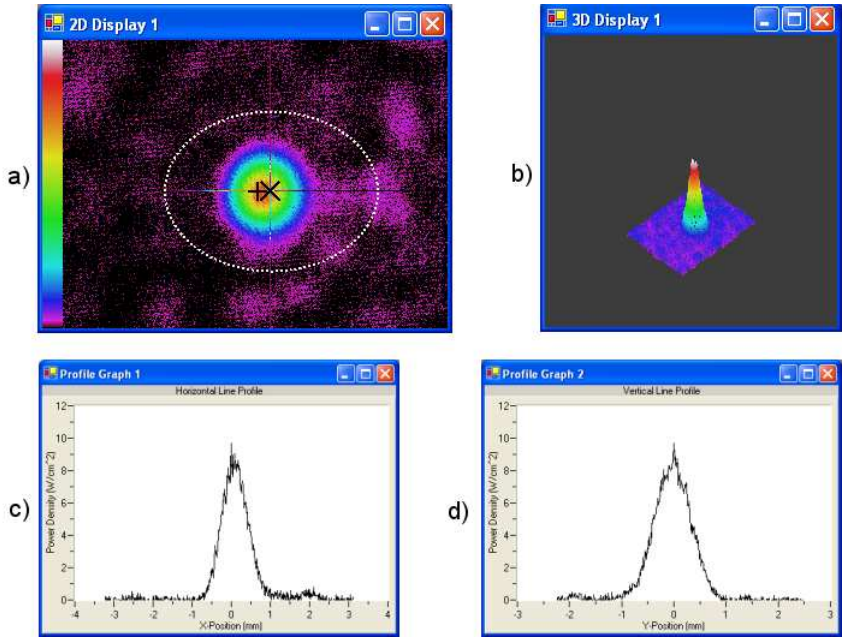

Figure 6.22: Laser spot: a) 2D image b) 3D image c) horizontal and d) vertical profile graph. Cavity length $L = 150$ mm, output power $P_{\text{out}} = 3.8$ W.

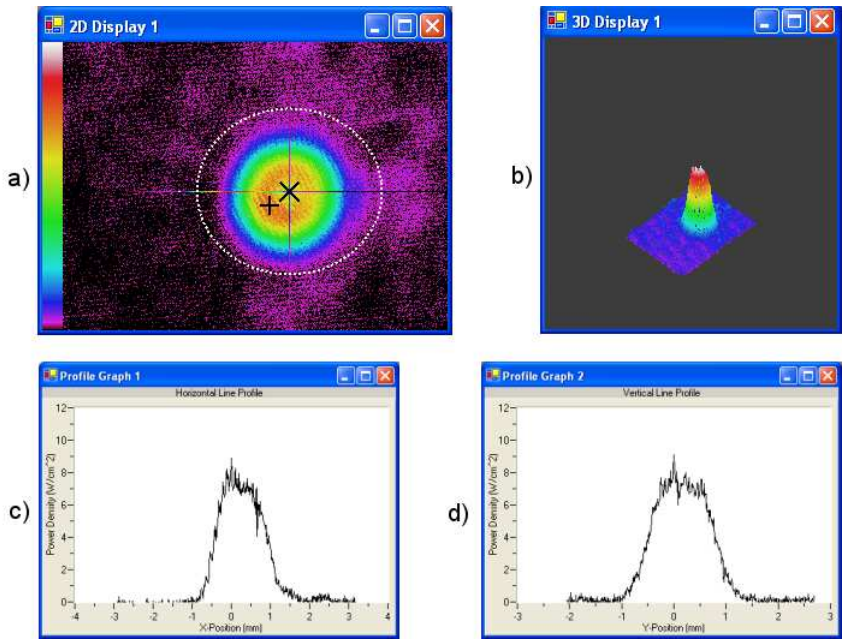

Figure 6.23: Laser spot: a) 2D image b) 3D image c) horizontal and d) vertical profile graph. Cavity length $L = 150$ mm, output power $P_{\text{out}} = 6.7$ W.

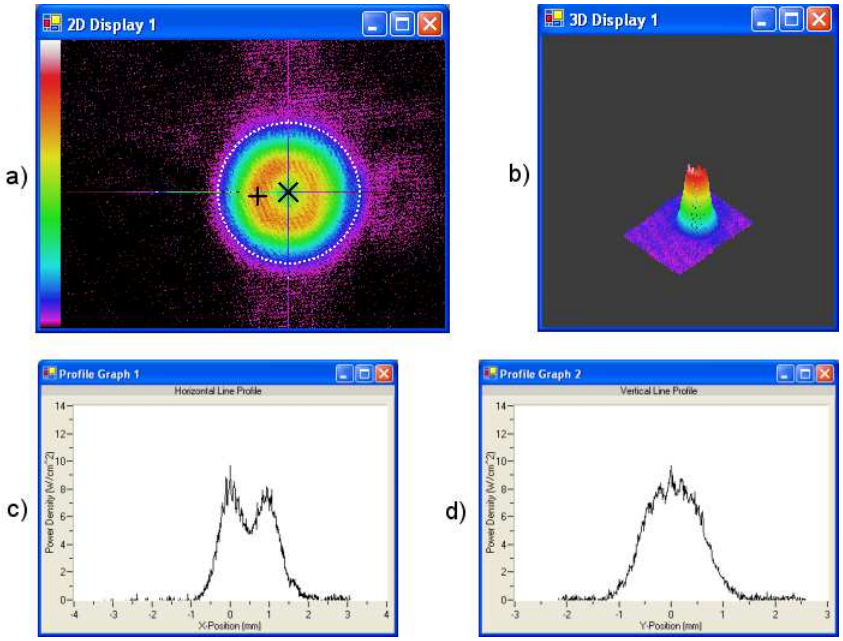

Figure 6.24: Laser spot: a) 2D image b) 3D image c) horizontal and d) vertical profile graph. Cavity length $L = 150$ mm, output power $P_{\text{out}} = 8.9$ W.

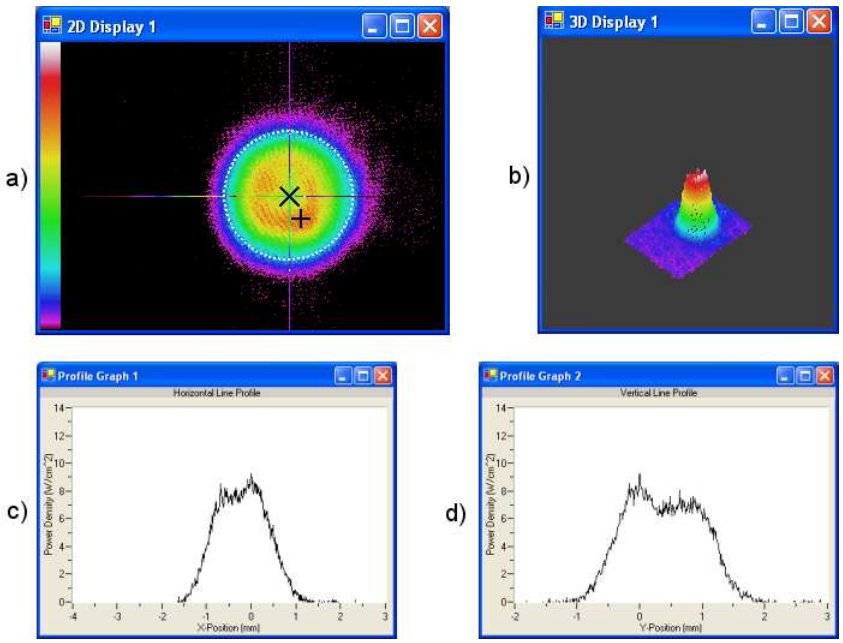

Figure 6.25: Laser spot: a) 2D image b) 3D image c) horizontal and d) vertical profile graph. Cavity length $L = 150$ mm, output power $P_{\text{out}} = 10.1$ W.

6.2.1 Results Analysis

The use of a smaller and longer active medium gave conflicting results. Slope efficiency is still high, up to 58%, but lasing threshold increased, leading to a lower wall-plug efficiency (see figure 6.21). Nevertheless, higher output powers can be reached before thermal lensing makes the cavity unstable. The camera screenshots do not show any apparent improvement in laser beam quality but the direct measurement of the M^2 shows a clear improvement, see table 6.5 and compare with table 6.3. With the 10 mm crystal, it was measured a M^2 varying from 2.8 up to 3.2 when the input power was increasing from 20.7 W to 24.8 W. With the 15 mm crystal a M^2 value of 2.8 was measured when the input power was 22.4 W. Therefore, these data confirms that heat removal is actually improved and so is the beam quality. Moreover, table 6.5 shows the interesting data of a much lower M^2 when the laser is operated in pulsed regime. This can probably be explained admitting that higher modes do not have time enough to gain and oscillate in the cavity. Table 6.6 shows even shorter pulses and higher peak powers than previously measured (cfr. table 6.4) and can likely be explained with a better alignment of the Q-switch.
So, at this stage, the 15 mm crystal seems to be a better choice than the 10 mm crystal in terms of beam quality, thanks to the better heat removal. A further simulation on a 3x3x10 mm^3 crystal (see fig. 6.26) shows how the temperature drop is actually entirely due to the smaller crystal cross section and not to the its longer dimension. It is therefore reasonable to argue that with such a crystal it should be possible to obtain a better beam quality without losing in efficiency.

6.3 Nd:$GdVO_4$ 3x3x15 mm^3

In order to evaluate the potentialities of Nd:$GdVO_4$ as gain medium, a 3x3x15 mm^3 crystal with 0.2 at. % dopant concentration was also purchased. The first face of the crystal is AR coated at 1064 nm and 808 nm, the second face is AR coated at 1064 and HR at 808 nm. The crystal was placed in the set-up described in section 6.2 in order to have comparable results with the

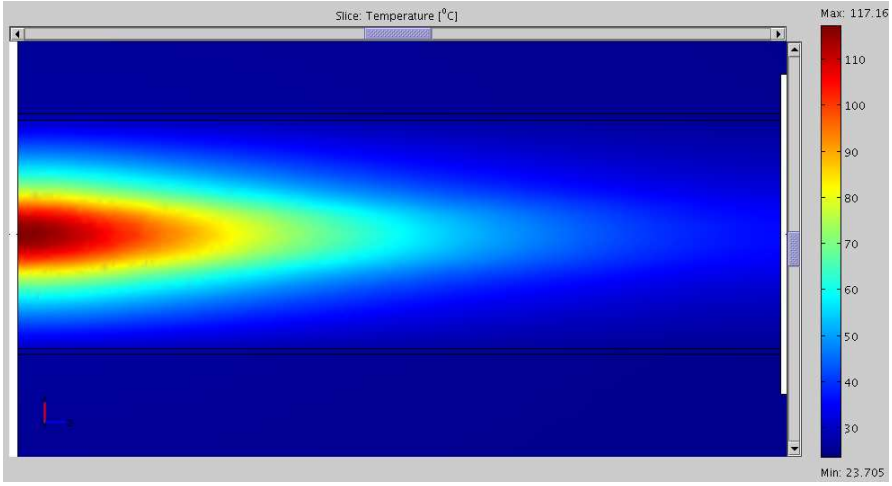

Figure 6.26: FEM simulation of temperature profile in a 3x3x10 mm^3 crystal.

f (kHz)	1	5	10	15	20	30	40	50	70
P_{av} (W)	1	4.3	6.8	7.7	8.1	8.9	9.4	9.8	10.1
τ (ns)	14	14.7	15.6	17.2	20.5	28.0	37.0	48.0	68.0
E_{i} (mJ)	1.00	0.86	0.68	0.51	0.41	0.30	0.24	0.20	0.14
P_{peak} (kW)	71.4	51.5	43.6	29.8	19.8	10.6	6.4	4.1	2.1
σ (%)	< 5	< 5	< 5	< 5	< 5	< 5	< 5	< 10	< 20

Table 6.7: Nd:GdVO$_4$ 3x3x15 mm^3: pulses properties at different working frequencies f. P_{av} is the average power, τ is the pulse FWHM, $E_{\text{i}} = P_{\text{av}}/f$ is the energy per pulse, $P_{\text{peak}} = E_{\text{i}}/\tau$ is a rough estimate of the pulse peak power and σ is pulse FWHM standard deviation.

yttrium vanadate host. A series of comparative graphs and tables is here presented.

6.3.1 Results Analysis

The advantage of the gadolinium host over the vanadate consists in the higher thermal conductivity. This should allow to reach higher output powers with a better beam quality. The first comparison, see figure 6.27, shows how the output power and slope efficiency of the two crystals are compara-

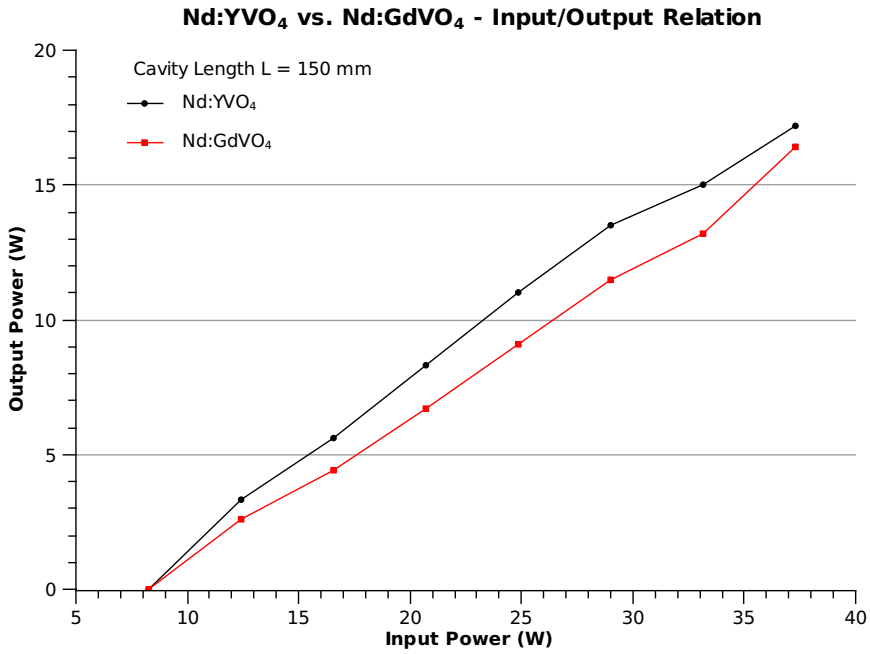

Figure 6.27: Laser input/output relation for gadolinium and vanadate crystals.

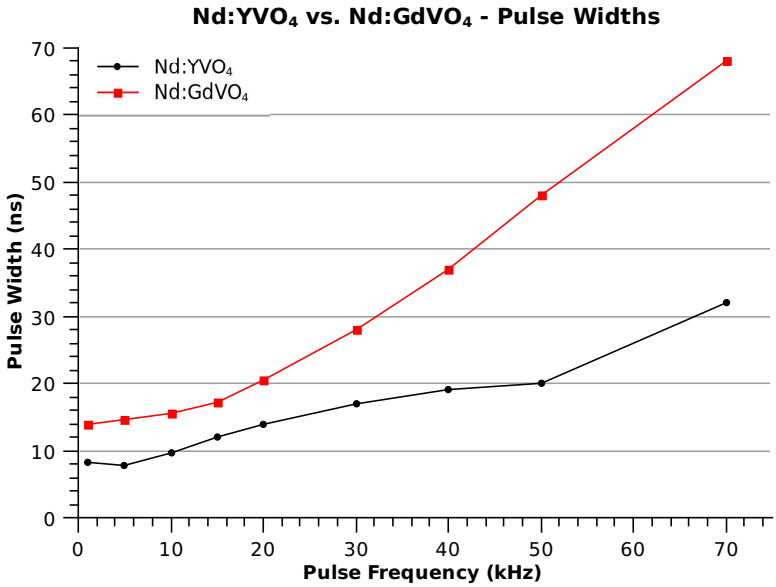

Figure 6.28: Comparison between Nd:YVO_4 and Nd:$GdVO_4$: pulse width

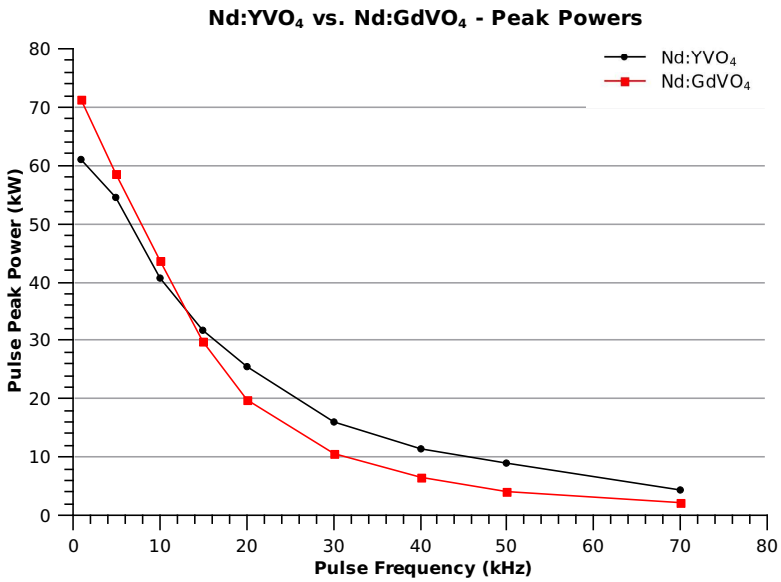

Figure 6.29: Comparison between Nd:YVO_4 and Nd:$GdVO_4$: pulses peak powers

ble, with yet a preference for the vanadate crystal. Measurements on the laser pulsed behavior (see table 6.7) were performed before measurements on the beam quality. The results on pulse width and pulse peak powers were not encouraging, see figures 6.28 and 6.29. The graphs clearly shows that the pulse width of the gadolinium host quickly rise with the working frequency, leading to peak powers lower than what could be achieved with the vanadate crystal. Gadolinium shows a behavior more similar to the YAG crystal, with high peak powers at low frequencies, rapidly decreasing at higher frequencies. This makes the gadolinium less suitable for fast marking application. These preliminary unfulfilling results lead to the decision to abandon further investigations on gadolinium host.

6.4 Sources Comparison

In order to have a full comparison among the different active media, a Nd:YAG crystal was placed in the same set-up and its pulsed behavior was measured as described in the previous sections. The YAG rod was 10 mm long and 4 mm wide in diameter. The measurements are summarized in table 6.8.

f (kHz)	1	5	10	20	40	60
P_{av} (W)	1.7	5.5	7.0	7.8	8.3	8.3
τ (ns)	15.7	16.8	24.0	42	62	112
E_{i} (mJ)	1.7	1.1	0.7	0.39	0.21	0.14
P_{peak} (kW)	108.3	65.5	29.2	9.3	3.4	1.2
σ (%)	< 5	< 5	< 5	< 10	< 20	< 30

Table 6.8: Nd:YAG: pulses properties at different working frequencies f. P_{av} is the average power, τ is the pulse FWHM, $E_{\text{i}} = P_{\text{av}}/f$ is the energy per pulse, $P_{\text{peak}} = E_{\text{i}}/\tau$ is a rough estimate of the pulse peak power and σ is pulse FWHM standard deviation.

f (kHz)	1	5	10	20	40	60
P_{av} (W)	1	5	10	18	20	20
τ (ns)	120	125	130	135	150	160
E_{i} (mJ)	1	1	1	0.9	0.5	0.33
P_{peak} (kW)	8.3	8.0	7.7	6.7	3.3	2.1

Table 6.9: Fiber Laser: pulses properties at different working frequencies f. P_{av} is the average power, τ is the pulse FWHM, $E_{\text{i}} = P_{\text{av}}/f$ is the energy per pulse and $P_{\text{peak}} = E_{\text{i}}/\tau$ is a rough estimate of the pulse peak power

Moreover, the average performances of 20 W fiber laser, manufactured by the American IPG and sold by SEI are shown, in order to have a full panorama of the available technologies. The pulsed behavior of the fiber laser are summarized in table 6.9.

Finally, it is possible to show in one single graph the main feature of the laser sources discussed so far, see figure 6.30. The graph clearly shows how the YAG crystal is not suitable for high frequency operations. Its optimal application field is where very high peak powers are needed, in spite of fast processing. Vanadate and gadolinium show a similar behavior, with yet a clear preference for the vanadate crystal at frequencies higher than 15 kHz, that is the range of our interest. The fiber laser, even with twice the average power of the other sources, due to its broad pulses, cannot reach the peak powers needed for our aims.

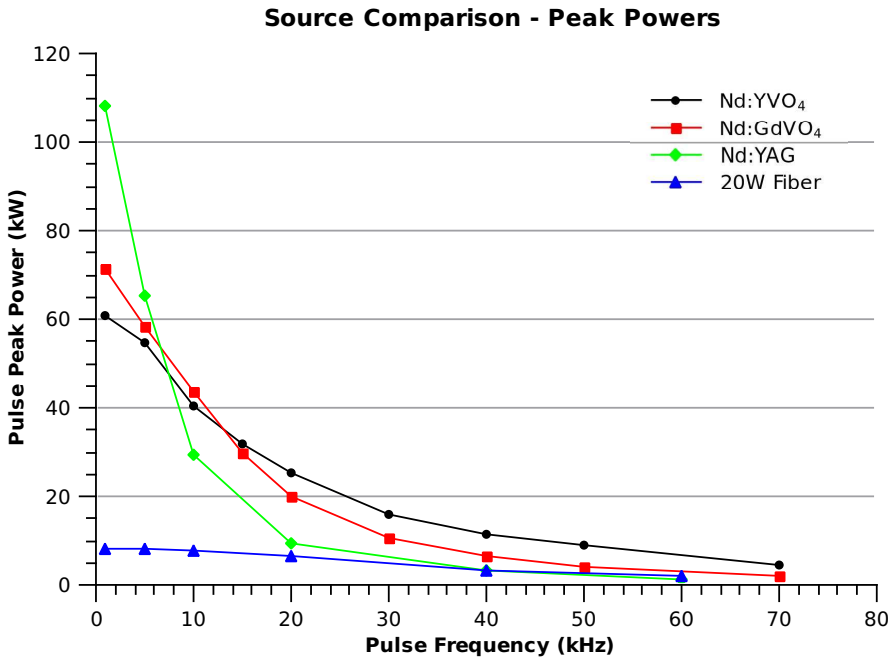

Figure 6.30: Comparison between several laser sources: pulses peak powers

Chapter 7

Conclusions and Future Developments

Purpose of this work was to develop a solid-state laser source, suitable for fast marking applications. Several requirements were to be satisfied:

- An output power of at least 10 W in continuous wave operation
- A low order mode beam: at least $M^2 < 2$
- Short pulses with high repeatability in Q-switched regime
- Air cooling
- Compact size

This work therefore concerned a theoretical and experimental study of laser generation in a solid-state active medium, with special insight on the most suitable gain medium and pump delivery optics and particular care for thermal effects. The theoretical analysis anticipated a few results:

- Nd:YVO_4 has to be preferred over the most widely used Nd:YAG, thanks to its peculiar physical properties, e.g., higher gain cross section, lower threshold, wider absorption bandwidth and polarized output.
- In order to extend thermal fracture limit, and therefore reach high output powers, a long and low doped crystal is necessary.

- Simple analytical formulas relating the pump beam quality and the active medium physical properties were derived. These formulas are a useful guidelines for designing the optical coupling system.

- Innocenzi's formula for theoretical calculation of thermal lens focal length is not accurate for high power systems, and needs to be corrected

While designing the laser source it was observed and decided that:

- A single-emitters fiber-coupled diode was the most suitable pump in order to have an optimal system industrialization, improved lifetime and low power consumption.

- Experiments proved the validity of equations (4.21) and (4.23) in predicting the lowest lasing threshold and the best beam quality. However,

- at high pump powers, a different set-up providing bigger pump waist has to be preferred, in order to reduce unfavorable thermal effects and to reach higher output powers.

- A simple, practical method to estimate the thermal lens focal length was found.

- The misalignment sensitivity was predicted and parametrized.

- A 10 mm long and low-doped (0.2 at. %) Nd:YVO_4 crystal was tested, according to previous considerations.

The experimental results showed that:

- A set-up cooled by a thermoelectric device can be as efficient as a more traditional water-cooled set-up, with the advantage of avoiding water circuits and bulky chillers. An optical-to-optical efficiency of 64% was reached for both the set-ups, with output power up to 20 W for short cavity length.

- The theories proposed by Fan et al. [23] were verified. A correction factor for Innocenzi's formula was empirically found. It appears that the dioptric power of the thermal lens-focal length has a linear dependence on the ratio between the laser beam size and the pump beam radius in the crystal.

- Simulations on crystal heating performed with the finite element method showed that a crystal with smaller cross section is cooled more efficiently while any further increase in the crystal length do not affect the temperature gradient. Moreover, the longer the crystal the higher the lasing threshold, with loss in efficiency. A suitable dimension was found to be 3x3x10 mm^3.

- Beam quality was found to be good at Q-switched operation, where $M^2 = 1.8$ was measured. This value guarantees a high quality and high efficiency processing. Yet, there is space for improvement, if a more suitable fiber is used in order to have a real "top-hat" pump beam.

- In Q-switched regime, the system proved to have high peak powers at high frequencies (approximately 9 kW at 50 kHz) and a very good pulse repeatability (standard deviation $< 5\%$)

- The comparison among other laser sources showed how the developed source is much more suitable for fast marking application than other more traditional technologies

7.1 Developments: the *Laser*^{3}

Further development of the prototype described in this work led to the commercialization of a compact, air-cooled laser source named *Laser*^{3}. The first machine was produced in December 2010, and had 12 W output power in continuous wave. One year later, a 20 W output power system was produces and commercialized. Hundreds unity have already been sold worldwide for a wide range of applications. High quality and reliability are the

Figure 7.1: Commercial solid-state laser machine by SEI

feature mostly appreciated by customers such as BTicino/LeGrand, Siropack (Marcegaglia Group), Roechling Automotive.

Further efforts were made in order to have a 40 W output power system, but the crystal thermal fracture limit was reached. The limitation was overcome with a MOPA concept. A master thesis studied the possibility to realize a frequency duplication in order to have green output radiation from the same laser cavity, see the work by M. Epis [1]. As this proved to be possible, more efforts are pushed in this direction.

Bibliography

[1] Michele Epis. Studio, progettazione e caratterizzazione di duplicatore di armonica applicato ad una sorgente laser nd:yvo$_4$ per applicazioni industriali. Master's thesis, Politecnico di Milano, 2010.

[2] T Frauenpreiss. Looking to higher power for laser speed?, 2005.

[3] Orazio Svelto. *Principles of Lasers*. Springer, 4th edition, 1998.

[4] Edoardo Capello. *Le lavorazioni industriali mediante laser di potenza*. Libreria Clup, 2003.

[5] A I Zagumennyi, V G Ostroumov, I A Shcherbakov, T Jensen, J P Meyn, and G Huber. The nd:gdvo$_4$ crystal: a new material for diode-pumped lasers. *Sov J Quantum Electron*, 22:1071, 1992.

[6] Y Sato and T Taira. Comparative study on the spectroscopic properties of nd:gdvo$_4$ and nd:yv0$_4$ with hybrid process. *IEEE J. Quantum Electron*, 11, 2005.

[7] foctek.net. http://www.foctek.net/products/crystals/nd_gdvo4.htm.

[8] William Koechner. *Solid-State Laser Engineering*. Springer, 5th edition, 1999.

[9] Pietro Pellegrini. Fresatura laser *nd* : *yag* di ottone: volume rimosso e rugosità in funzione dei parametri di processo. Master's thesis, Politecnico di Milano, 2008.

[10] J Kong, D Y Tang, S P Ng, L M Zhao, L J Qin, and X L Meng. High-power diode-end-pumped cw nd:gdvo$_4$ laser. *Opt Laser Technol*, 37:51–54, 2004.

[11] J Liu, Z Shao, H Zhang, X L Meng, L Zhu, and M Jiang. High-power end-pumped cw nd:gdvo$_4$ laser formed with a flat–flat cavity. *Opt Laser Technol*, 31:459–62, 1999.

[12] Y-F Chen. Design criteria for concentration optimization in scaling diode end-pumped lasers to high powers: influence of thermal fracture. *IEEE J. Quantum Electron*, 35(2):234–239, February 1999.

[13] M Tsunekane, N Taguchi, T Kasamatsu, and H Inaba. Analytical and experimental studies on the characteristics of composite solid-state laser rods in diode-end-pumped geometry. *IEEE J. Select. Topics Quantum Electron.*, 3:9–18, 1997.

[14] S C Tidwell, J F Seamans, M S Bowers, and A K Cousins. Scaling cw diode-end-pumped nd:yag lasers to high average powers. *IEEE J. Quantum Electron*, 28:997–1009, 1992.

[15] T Sasaki, T Kojima, A Yokotani, O Oguri, and S Nakai. Single-longitudinal-mode operation and second-harmonic generation of nd:yvo$_4$ microchip lasers. *Opt. Lett.*, 16:1665–1667, 1991.

[16] A K Cousins. Temperature and thermal stress scaling in finite-length end-pumped laser rods. *IEEE J. Quantum Electron*, 28:1057–1069, 1992.

[17] Y-F Chen, C F Kao, and S C Wang. Analytical model for the design of fiber-coupled laser-diode end-pumped lasers. *Opt. Comm,*, 133:517–524, 1997.

[18] F Hajiesmaeilbaigi, A Koohian, and M Mahdizadeh. Design criteria in fibre-coupled end-pumped laser with small active medium. *J. Opt. A: Pure Appl. Opt.*, 4:52–56, 2002.

[19] P Laporta and M Brussard. Design criteria for mode size optimization in diode-pumped solid-state lasers. *IEEE J. Quantum Electron*, 27(10):2319–26, December 1991.

[20] Y-F Chen, T M Huang, C F Kao, C L Wang, and S C Wang. Optimization in scaling fiber-coupled laser-diode end-pumped lasers to higher power: influence of thermal effect. *IEEE J. Quantum Electron*, 33(8):1424–29, August 1997.

[21] V Magni. Resonators for solid-state lasers with large-volume fundamental mode and high alignement stability. *Applied Optics*, 25(1):107–117, January 1986.

[22] M E Innocenzi, H T Yura, C L Fincher, and R A Fields. Thermal modeling of continous-wave end-pumped solid-state lasers. *Appl Phys Lett*, 56(19):1831–33, May 1990.

[23] S Fan, X Zhang, Q Wang, S Li, S Ding, and F Su. More precise determination of the thermal lens focal length for end-pumped solid-state lasers. *Opt. Comm,*, 266:620–26, 2006.

[24] X Peng, L Xu, and A Asundi. Power scaling of diode-pumped nd:yvo$_4$ lasers. *IEEE J. Quantum Electron*, 38(9):1291–99, September 2002.

[25] X Peng, A Asundi, Y Chen, and Z Xiong. Study of the mechanical properties of nd:yvo$_4$ crystal by use of laser interferometry and finite-element analysis. *Applied Optics*, 40(9):1396–1403, March 2001.